MEASUREMENT OF EXCITATION FUNCTIONS OF NEUTRON INDUCED REACTIONS IN THE ENERGY RANGE 13-15 MeV USING D-T NEUTRON SOURCE AT NEUTRON GENERATOR

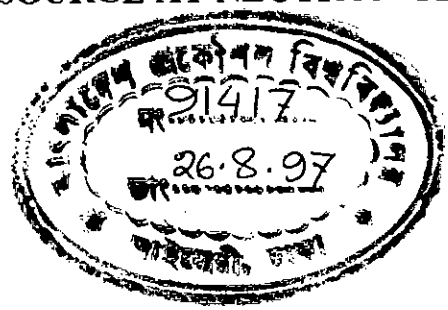

BY

SYED MOHAMMOD HOSSAIN

Roll No. : 9010p
Registration No. : 88102
Session : 1988-89

A thesis submitted to the Department of Physics
in partial fulfillment of the requirements for the degree of
Master of Philosophy in Physics

BANGLADESH UNIVERSITY OF ENGINEERING AND TECHNOLOGY
Dhaka, Bangladesh.

JULY, 1997

BANGLADESH UNIVERSITY OF ENGINEERING AND TECHNOLOGY, DHAKA

DEPARTMENT OF PHYSICS

Certification of Thesis on

Measurement of excitation functions of neutron induced reactions in the energy range 13-15 MeV using D-T neutron source at neutron generator.

BY

SYED MOHAMMOD HOSSAIN

has been accepted as satisfactory in partial fulfilment for the degree of Master of Philosophy in Physics and certifying that the student demonstrated a satisfactory knowledge of the field covered by this thesis in an oral examination held on August 14, 1997.

Board of Examiners

1. Prof. Gias uddin Ahmad
   Department of Physics
   BUET, Dhaka.
   ..... **Supervisor** 14-08-97

2. Dr. N. I. Molla
   Director, INST
   AERE, Savar, Dhaka
   ..... 14.8.97 ..... **Co-Supervisor**

3. Prof. Mominul Huq
   Head
   Department of Physics
   BUET, Dhaka.
   ..... 14.08.97 ..... **Member**

4. Prof. H. M. Sengupta
   Department of Physics
   University of Dhaka
   Dhaka.
   ..... 14.8.97 ..... **Member (External)**

DECLARATION

This thesis has been done by the candidate himself and does not contain any material extracted from elsewhere or from a work published by any body else. The work of this thesis has not been presented by the candidate for another degree or diploma in any other University. No other person's work has been used without due acknowledge.

(Syed Mohammod Hossain)

Candidate

CERTIFICATE

This is to certify that the research work embodying this thesis has been carried out under our supervision in the Neutron Activation Analysis (NAA) Laboratory, Institute of Nuclear Science and Technology, Bangladesh Atomic Energy Commission, Dhaka. The research work presented herein is original. This thesis has not been submitted for the award of any other degree or diploma in any other University.

(Dr. Gias Uddin Ahmad)

Supervisor
Professor
Department of Physics
Bangladesh University of
Engineering and Technology

(Dr. N.I. Molla)

Co-Supervisor
Director & Chief Scientific Officer
Institute of Nuclear Science & Technology
Bangladesh Atomic Energy Commission

Dedicated

To My

Mother

Abstract

Excitation functions for the (n,α) reaction on ^{63}Cu isotope and the (n,2n) processes on ^{35}Cl, ^{100}Mo and ^{140}Ce isotopes have been measured over the neutron energy range of 13.82 - 14.71 MeV. Activation technique has been used in the measurement. The target elements were exposed to D-T neutrons produced by bombarding a air cooled, 3.7×10^{11} Bq copper backing tritium target with a 110 keV deuteron beam (d^+) at the J-25 (AID, France) neutron generator facility of the Institute of Nuclear Science & Technology. For characterization of ^{34m}Cl, ^{60}Co, ^{99}Mo, and ^{139}Ce radioisotopes, high resolution gamma-ray spectrometry was applied. Monitor reaction $^{93}Nb(n,2n)^{92m}Nb$ was used for the neutron flux measurement of $^{63}Cu(n,\alpha)^{60}Co$ reaction while monitor reaction $^{27}Al(n,\alpha)^{24}Al$ was used for the flux measurement of (n,2n) processes on ^{35}Cl, ^{100}Mo and ^{140}Ce isotopes. The cross section values obtained from the available literature data have been plotted as a function of neutron energy to get the excitation functions of the reactions. Statistical model calculations were performed to reproduce the excitation functions of $^{63}Cu(n,\alpha)^{60}Co$ and $^{100}Mo(n,2n)^{99}Mo$ reactions using statistical code SINCROSS-II . Statistical code EXIFON was used in the case of $^{100}Mo(n,2n)^{99}Mo$ and $^{140}Ce(n,2n)^{139}Ce$ reactions. In most cases the experimental and theoretical results were found to be in good agreement.

Acknowledgement

It is a great pleasure for me to acknowledge my deepest sense of gratitude and indebtedness to my reverend teachers and supervisors Professor Gias Uddin Ahmad, Department of Physics, Bangladesh University of Engineering & Technology and Dr. Nurul Islam Molla, Director and Chief Scientific Officer, Institute of Nuclear Science & Technology (INST), Atomic Energy Research Establishment (AERE) for their indispensable guidance, untiring efforts and constant encouragement at all stages of this work.

I am greatly obliged to Professor S.M. Qaim, Institut fur Nuklearchemie, Forschungszentrum, Julich, Federal Republic of Germany for his helpful comments, inciting discussions and significant suggestions in the experimental work during his visit to INST as an IAEA Expert. I am also indebted to Dr. Y. Ikeda, Dr. Satoshi Chiba, and Y. Fukahori of Nuclear Data Centre, Japan Atomic Energy Research Institute for their helpful suggestion and valuable advice for the theoretical calculation of activation cross section using the code SINCROSS-II.

I am extremely delighted to express my indebtedness and thankful acknowledgement to Dr. M. Mizanur Rahman, Chief Scientific Officer and Head, Nuclear and Neutron Physics Division, INST, AERE for his stimulating discussions and experimental assistance throughout the progress of the work.

I do express my gratitude's to Md. R.U. Miah, PSO, M.N. Islam, SSO, M.S. Basunia, SO, M.A. Hafiz, AE of INST, AERE for their invaluable help and friendly cooperation at different stages of this work. I am also grateful to the Neutron Generator Operation Group for providing me with deuteron beam and Mr. Ahad Ali, RA for their help and cordiality.

I cannot but express my every gratitude and indebtedness to my mother and brothers whose sacrifice and blessing have made it possible to carry out my study.

My grateful thanks to my wife, Rubaiyat Jahan Biswas, Lecturer in Psychology, Dhaka Commerce College for her inspiration and understanding during my study.

Content

			Page
Chapter-1		Introduction	1
Chapter-2		Theory and Experimental Set-up of Neutron Activation Analysis (NAA) Technique	7
	2.1.	Theory of Neutron Activation Analysis (NAA)	7
	2.1.1.	General consideration of NAA	7
	2.1.2	Method of NAA	9
	2.2.	Experimental set up of Neutron Activation Analysis	12
	2.2.1.	Irradiation Facility	12
	2.2.2.	Gamma-ray Spectrometry System	13
	2.2.2.1.	The Detector	14
	2.2.2.2.	Electronics and Software	18
	2.2.2.3.	Detector Response	21
	2.2.2.4.	Peak Position and Area	22
Chapter-3		Study of the Detector Parameters	24
	3.1.	Chi-square Test of HPGe Detection System	24
	3.2.	Energy Resolution of HPGe Detector	26
	3.3.	Energy Calibration of HPGe Detector	28
	3.4.	Efficiency Calibration of HPGe Detector	29

Contents

			Page
Chapter-4		Excitation Function Measurements of $^{63}Cu(n,\alpha)^{60}Co$ Reaction in the Neutron Energy Range 13.82 - 14.71 MeV	35
	4.1.	Introduction	35
	4.2.	Experimental Procedure	37
	4.2.1.	Neutron Source	37
	4.2.2.	Samples	37
	4.2.3.	Irradiation	38
	4.2.4.	Neutron Flux Monitor	39
	4.2.5.	Gamma-ray Measurement	39
	4.2.6.	Cross Section Calculation and Error Estimation	41
	4.3.	Results and Discussion	41
Chapter-5		Excitation Functions of (n,2n) Processes on Some Isotopes of Cl, Mo, and Ce in the Energy Range 13.90 - 14.71 MeV	44
	5.1.	Introduction	44
	5.2.	Experimental Procedure	46
	5.2.1.	Sample Preparation and Irradiations	46
	5.2.1.1.	Irradiation of NaCl Samples	46
	5.2.1.2.	Irradiation of Mo_2O_3 Samples	47
	5.2.1.3.	Irradiation of CeO_2 Samples	48
	5.2.2.	Neutron Flux Monitor	48
	5.2.3.	Activity Measurements	49

Contents

			Page
	5.2.4.	Cross section Calculation and Error Estimation	49
	5.2.5.	Nuclear Model Calculation	50
	5.3.	Results and Discussion	50
Chapter-6		Theoretical Calculation Codes for Activation Cross Section Evaluation in the Neutron Energy Range 13 - 15 MeV.	57
	6.1.	Introduction	57
	6.1.1.	SINCROSS-II - A Nuclear Cross Section Calculation System with Simplified Input Format	59
	6.1.1.1	Introduction	59
	6.1.1.2.	Optical Model Potential Parameters	59
	6.1.1.3.	Level Density and Gamma-ray Transition Parameters	60
	6.1.1.4.	Determination Procedure for the Value of Parameters	62
	6.1.1.5.	Parameter Determination of the Pre-equilibrium Processes.	63
	6.1.1.6.	Parameter Determination of the Level Density	63
	6.1.1.7.	Calculation of Activation Cross Section using EGNASH2 and Comparison between Calculated and Experimental Values.	64
	6.1.2.	EXIFON - A Statistical Multistep Direct And Multistep Compound Reaction Model	66
	6.1.2.1	Introduction	66
	6.1.2.2.	The Statistical Multistep Reaction Model	67

	6.1.2.3.	Activation Cross Sections	67
	6.1.2.4.	Model Parameters of EXIFON	69
	6.1.2.5	Statistical Multistep Direct (SMD) Cross Sections	71
	6.1.2.6.	Statistical Multistep Compound (SMC) Cross Sections	72
	6.1.2.7.	General Features and Standard Parameter Set of EXIFON	74
Chapter-7		Conclusions	76
Chapter-8		References	77

CHAPTER-1

INTRODUCTION

Introduction

The series of facts tied together by the 'neutron' began in 1930 when Bothe and Beaker bombarded beryllium with polonium alphas and found a very penetrating but non-ionizing radiation; they logically assumed that it was a gamma-ray. In 1932, Chadwick assumed that the "beryllium radiation" was not a gamma-ray but was formed of neutral particles of closely protonic mass, i.e., 'neutrons' which can not be accelerated in electric or uniform magnetic fields. This discovery opened up a vast field for further experimental work.

Since its discovery, neutron has been playing an important role to build up the scope and importance of nuclear reactions, nuclear structure and in the advancement of nuclear technology. The many nuclear reactions induced by neutron have formed a valuable source of information about the nucleus, and have produced many new nuclear species. These artificially made nuclides yield further information about nuclei, and have applications in other branches in science, such as chemistry, biology and medicine. The most striking use of neutrons is in the chain reactions involving fissile materials. The development of fission reactor was made possible by Otto Hahn et. al.[1] with the discovery that heavy nuclei can be fissioned by neutrons.

Fusion energy reactors will be based upon the $T(d,n)^4He$ reaction. In D-T fusion almost 80% of the total energy is carried off by 14 MeV neutrons[2]. The accurate knowledge of neutron interaction cross-sections around 13-15 MeV energies are of strong interest for fusion facilities. Nowadays, neutron production from plasma is of reality, which makes the nuclear data to have special usefulness to monitor plasma temperature and to assess D-T fuel "burn" rates during the containment intervals. Of concern for blanket design purpose, are tritium breeding cross-sections and neutron multiplier cross-sections for energies of about 14 MeV and below. Of larger range concern are such matters as radiation damage by energetic neutrons and long-lived activation of fusion structure. These are important matters which

will affect the longevity and service of facilities and decommissioning procedures. Sophisticated accelerators, high sensitive detection system, advanced radiochemical methods and high speed computing machines have given added impetus to research workers worldwide to study these reactions.

About one third of the total elements available in nature are considered in one form or another as structural materials of fusion reactor. Therefore, precise measurements of activation cross-section as a function of neutron energy of these structural materials around 13-15 MeV neutrons are of considerable interest for validation support as well as for practical applications, especially for calculations of nuclear transmutation rates, nuclear heating, nuclear dosimetry, radiation damage due to gas formation in the potential first wall materials, radiation shielding, isotope production, energy deposition in the first wall, superconducting magnet induced activity and so on.

Any nuclear transmutation process may lead to an excited state of the product nucleus, and the decay of the excited state then gives information about energy levels and decay schemes. Different reaction channels such as, (n,p), (n,2n), (n,α), (n,n$'$), etc. open to the interaction of neutron with target materials. The data on (n,2n) reactions are important for calculating the neutron multiplication, (n,p) and (n,α) reactions for evaluating the radiation damage.

The techniques used in the determination of reaction cross-sections around 14 MeV neutrons are divided into three groups; spectrum method, gas accumulation method and activation method. The measurements of nuclear reaction cross-sections by the use of spectrum method is rather difficult because it needs the study of the spectra of emitted particle and angular distributions in a high background radiation. However, this method provides useful information regarding the mechanism of the nuclear reactions. The spectrum method is not sensitive to identify the low-abundance emitted particles. On the other hand, a modified activation technique consists of accumulation and integral measurements of the emitted particles.

Since its discovery in 1936 by G. Hevesy and H. Levi, Neutron Activation Analysis (NAA) technique has progressed rapidly and has become today a versatile and sensitive analytical tool in all branches of science and technology. Rapid advances in nuclear techniques have enabled scientists to use this technique as an effective tool for activation cross section measurements.

The fundamental principles on which activation analysis is based have remain unchanged, but the tremendous development which have taken place in the last decades in electronic equipment in general and in detection instrumentation (such as, HPGe, Si detector) in particular, gave impetus to this technique.

NAA is being used extensively for the measurements of nuclear reaction cross-section data around 14 MeV neutron for the following advantages: high sensitivity, good resolution, low background and the probability of automation and bulk media assay. However, NAA is limited by the following factors: low isotopic abundance, low flux, low reaction cross-section, short irradiation time due to finite target life, low gamma intensity and the interference from the radiation produced in the heavier isotopes.

Different types of neutron generator producing monoenergetic neutrons through D-D and D-T reactions are in use around the world with a view to facilitating research on nuclear reactor technology. A SAMES J-25 AID (France) neutron generator was installed at the Institute of Nuclear Science & Technology (INST), Atomic Energy Research Establishment (AERE), Savar, Dhaka under the coordinated research program with the IAEA for the measurements of nuclear data. In J-25 neutron generator , 14 MeV monoenergetic neutrons are produced via $^{3}H(d,n)^{4}He$ reaction. The large positive Q-value (17.6 MeV) and low atomic number make it possible to produce 14 MeV neutrons even at low deuteron incident energies, e.g., E_d = 100-200 keV. This intense neutron source is, therefore, being used for the investigation of the interaction of fast neutrons with potential structural materials of nuclear reactors which are important for the design, development, safe operation of fission and fusion reactors.

Cross-section data as a function of neutron energy provide excitation function for the reaction. Therefore, it is essential to place the samples in a well defined position with respect to the direction of the deuteron beam which in turn corresponds to emitted neutron energy, both for activation and prompt radiation analysis as well as for neutron nuclear data measurements around 14 MeV. The energy of the incident neutron depends on the bombarding deuteron energy (E_d) and the emission angle (θ). For high threshold reaction , the activity depends on both on the position and dimension of the sample. The energy distribution of neutron produced by D-T reaction in J-25 neutron generator as a function of emission angle with respect to the direction of deuteron beam was measured by the ratio of ^{90}Zr and ^{92m}Nb specific activities produced in them by (n,2n) reaction[3]. The (n,2n) cross-section of ^{90}Zr varies rapidly with neutron energy around 14 MeV while that for $^{93}Nb(n,2n)^{92m}Nb$ shows negligible change and thus it permits to measure the average neutron energy versus emission angle at different position.

Analysis of literature data shows that a large number of experimental neutron cross section data around 14 MeV have been reported and great efforts were initiated on their compilations and evaluations but there are often unexplained inconsistencies among the existing experimental data[4-6].

The extent of deviations in the cross-section values of a particular reaction measured by different authors can be estimated by the following example: Prasad et al.[7] measured the cross-section for $^{35}Cl(n,2n)^{34m}Cl$ reaction at 14.8 MeV using the activation technique and reported σ = 12.00 mb while Scalan et al.[8] obtained σ = 5.6 mb for the same reaction using the same technique. Similarly, in the measurement of cross-sections for $^{100}Mo(n,2n)^{99}Mo$ reaction a cross-section value of $\sigma = 1134\pm29$ was reported by Khalda et.al.[9] with the use of activation technique but M. Lederer et.al.[10] reported $\sigma = 390\pm60$ mb for the same reaction at the same neutron energy and technique.

Benard[6] has reported the compilation and evaluation of 14 MeV neutron activation cross sections on the selected reactions. He discussed the problem and showed the useful method to confirm the range of the accuracy in the available data. However, there is still uncertainty in terms of correlations between different reaction cross section data measured at different neutron fields. The main source of discrepancy in the experimental data is attributable to the difference of the experimental conditions (the neutron source characteristics, radiation measuring technique, neutron monitoring method), standard cross-section data and decay data (gamma-ray branching ratio, half-life, natural abundance). Thus a new systematic experiment is needed basing on the same experimental configuration covering wider range of reaction.

From this point of view, a program of activation cross section measurements for fusion reactor structural materials around 14 MeV neutrons has been continuing using Fast Neutron Source (FNS) facility since 1986 at the Institute of Nuclear Science & Technology, Savar, Dhaka under the coordinated Research Program (CRP) with IAEA. In this experimental program a large number of reaction cross section have been measured in our laboratory on the same experimental condition[11]. In the present work four reactions $^{35}Cl(n,2n)^{34m}Cl$, $^{63}Cu(n,\alpha)^{60}Co$ $^{100}Mo(n,2n)^{99}Mo$ and $^{140}Ce(n,2n)^{139}Ce$ have been studied experimentally and model calculations have been performed for these reactions using statistical codes EXIFON and SINCROSS-II for the first time in our laboratory.

The activation cross section for $^{63}Cu(n,\alpha)^{60}Co$ reaction is of continuing interest in reactor dosimetry as a long-term fast neutron fluence monitor[12]. The convenient residual product decay permits accurate detector calibration for gamma detection and sample foils are readily available with sufficient purity. The nuclear data requirements for fusion energy development summarized in a number of papers[13] indicate that the measurements of activation cross-sections for $^{63}Cu(n,\alpha)^{60}Co$ reaction have priority for dosimetry, too[14].

The (n,2n) cross-section data in the case of structural materials of a fusion reactor are important for the estimation of neutron multiplication and neutron transmutation. But the

data that are available for such reactions around 14 MeV are often contradictory especially in the case of $^{35}Cl(n,2n)^{34m}Cl$, $^{100}Mo(n,2n)^{99}Mo$ and $^{140}Ce(n,2n)^{139}Ce$ reactions. Furthermore, activation cross section for such reactions are also needed for waste disposal assessment of fusion reactor materials.

A general survey of the existing literature for the reactions $^{63}Cu(n,\alpha)^{60}Co$[15-23], $^{35}Cl(n,2n)^{34m}Cl$[7,8,24-28], $^{100}Mo(n,2n)^{99}Mo$[9,10,24,27,29-32], and $^{140}Ce(n,2n)^{139}Ce$[17,19,20,28,33-34] show that the reaction cross-section data around 14 MeV are either sparse or, if available, are often in disagreement with one another. To overcome these discrepancies we chose to study the excitation functions of the reaction of $^{63}Cu(n,\alpha)^{60}Co$, $^{35}Cl(n,2n)^{34m}Cl$, $^{100}Mo(n,2n)^{99}Mo$, and $^{140}Ce(n,2n)^{139}Ce$ in the neutron energy range 13.82-14.71 MeV using the neutron generator facility of INST, AERE, Savar. Dhaka.

The theoretical cross-sections as a function of neutron energy have been calculated for the $^{63}Cu(n,\alpha)^{60}Co$, $^{100}Mo(n,2n)^{99}Mo$ and $^{140}Ce(n,2n)^{139}Ce$ reaction using the computer code EXIFON[35] and SINCROSS-II[36].

CHAPTER-2

THEORY AND EXPERIMENTAL SET-UP OF NEUTRON ACTIVATION ANALYSIS

Theory and Experimental set up of Neutron Activation Analysis (NAA) Technique

2.1. Theory of Neutron Activation Analysis (NAA)

2.1.1. General Consideration of NAA

Since its discovery in 1936 by G. Hevessy and H. Levy, neutron activation analysis (NAA) has progressed rapidly and has become today a versatile and sensitive analytical tool in all branches of science and technology[37]. Based on the highly characteristic and well defined nuclear properties of the elements, this technique is close to an ideal non-destructive analytical method, capable of handling samples in liquid, solid, or powder form.

The theory of NAA is based on a nuclear reaction. Nuclear reactions are used to product radionuclides or excited states of the target nucleus as the basis for analytical determination. When a neutron interacts with a target nucleus, a compound nucleus is formed. The compound nucleus has a certain finite life time (10^{-13} - 10^{-15} sec) during which it remains in a highly excited state due to the high binding energy and kinetic energy of the neutron in the nucleus. De-excitation of the compound nucleus can occur in different ways that are independent of the way the compound nucleus is formed. Each of these process (figure-2.1) has a certain probability, depending on the nuclear cross-section of each mode, which is related to the excitation energy of the compound nucleus.

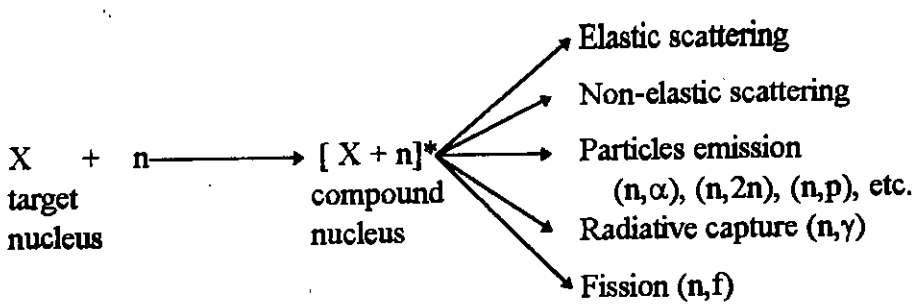

Figure.2.1. Reaction kinematics.

In elastic scattering the resulting nucleus is identical with the target, whereas in non-elastic scattering a radioactive isomer may be formed. In the emission of particles the resulting nuclide is usually radioactive and differs from the target nuclide in atomic or mass number, or both. In radiative capture the excited nucleus passes to a lower energy state by the emission of one or more gamma-rays. The resulting nuclide is usually radioactive. In fission the excited nucleus splits into two nuclei accompanied by the emission of neutrons and gamma-rays. The fission process is limited to only a few elements with atomic numbers ($Z>82$)[38].

A radioactive nuclide has a characteristic half-life ($t_{1/2}$) mode of decay and energy of emitted radiation during the decay process. Depending on the energy considerations (Q-value), a radionuclide can decay to a daughter product (usually stable) by various ways.

Most of the radionuclides that undergo decay by alpha, beta, or positron emission and by electron capture also emit gamma-rays as a result of readjustment of energy content in the radionuclides during their transition from excited states to more stable states. Gamma-ray measurements have, in general, much wider applications in NAA because gamma-rays emitted from the most radionuclides have a wider range of energies and have large penetrating range and thus are subject to minimal loss by absorption in a sample matrix during their measurements. This property coupled with the developments in high resolution and high efficiency semiconductor detectors such as High Purity Germanium (HPGe) detectors and the availability of high neutron flux reactors, neutron generator, etc., make NAA gamma spectrometry a powerful technique in measuring activation cross-section and multielemental determination in various type of samples.

2.1.2. Method of NAA

NAA methods are usually divided into three categories depending on whether any chemical separations are required during the course of experiment. If preirradiation chemical separations are required, the technique is termed chemical NAA (CNAA). If post irradiation chemical separation are performed the technique is called radiochemical NAA (RNAA). If no chemical separations are needed, the process is called INAA. In the present experiment only INAA technique was used.

NAA methods can also be grouped by the energy of neutrons used in irradiation process. For example, if slow, or thermal neutrons are used in the irradiation process (i.e, neutrons with velocities about 2200 ms^{-1}), the activation analysis is called thermal neutron activation analysis. Other methods include epithermal and fast neutron activation analysis. Epithermal neutrons have energies between 0.5 eV and 1 keV, and fast neutrons are classified as those having energies greater than 0.5 MeV.

As stated previously , once an element is bombarded with a neutron, a compound nucleus is formed and different reaction channel such as elastic and inelastic, (n,p), (n,2n) and (n,f), etc. may open. The time rate of change $dN^*(t_i)/dt$, of radioactive nuclei during activation, is dependent on the number of original parent nuclei, N, neutron flux, ϕ, nuclear reaction cross-section to be determined in the present experiment, σ. The number of activated nuclei over irradiation time , $N^*(t_i)$, and the parameters described above are expressed by the following relationship[39)]

$$\frac{dN^*(t_i)}{dt} = N\phi\sigma - \lambda N^*(t_i) \qquad \text{.....(2.1)}$$

where λ is the decay constant and is related to the half-life of N* by the following formula

$$\lambda = \frac{\ln 2}{t_{\frac{1}{2}}} \qquad \text{.....(2.2)}$$

A time dependent equation can be solved for by using differential equations. The result is

$$N^*(t_i) = \frac{N\phi\sigma}{\lambda}(1 - e^{-\lambda t_i}) \qquad \text{.....(2.3)}$$

where t_i is the irradiation time. As irradiation time become increasingly longer (longer than 6-7 half-lifes), the number of radioactive nuclei, N^*, reaches its saturation limit due to the constant loss of radioactive nuclei to decay. This limit is represented below by the equation for $N^*(t_i)$

$$N^*_{sat} = \frac{N\phi\sigma}{\lambda} \qquad \text{.....} \quad (2.4)$$

After irradiation , the source of N* is gone and the nuclei are left only to decay. The number of radioactive nuclei after irradiation and decay can then be described by,

$$N^*(t_i, t_d) = N^*(t_i)\ e^{-\lambda t_d} \qquad \text{.....(2.5)}$$

where t_d is the decay time. The expression for $N^*(t_i)$ from equation (2.3) can be substituted in to the equation (2.5) to get the following expression for $N^*(t_i,t_d)$

$$N^*(t_i, t_d) = \frac{N\phi\sigma}{\lambda}(1 - e^{-\lambda t_i})\ e^{-\lambda t_d} \qquad \text{.....(2.6)}$$

After a decent cooling time, the sample is counted using a HPGe detector. The change in number of radioactive elements during the decay time can be expressed by the rate equation below

$$\frac{dN^*(t_i,t_d,t_c)}{dt} = N^*(t_i,t_d) - \lambda N^*(t_i,t_d,t_c) \quad \text{..... (2.7)}$$

Solving this equation, the number of radioactive nuclei emitting gamma-rays during the counting period, $N^*(t_i,t_d,t_c)$, can be described by the following relation,

$$N^*(t_i,t_d,t_c) = \frac{N\phi\sigma}{\lambda}(1-e^{-\lambda t_i})\ e^{-\lambda t_d}(1-e^{-\lambda t_c}) \quad \text{.....(2.8)}$$

The detector can not detect all the gamma-rays emitted by the sample simply due to the fact that the detector crystal is limited in size and geometry. The reaction probability depends on the gamma-ray energy, crystal size and counting geometry. The total number of emitted gamma-rays that will actually be detected is much lower than the number actually emitted, and is equal to

$$C^*(t_i,t_d,t_c) = \frac{N\phi\sigma}{\lambda}(1-e^{-\lambda t_i})\ e^{-\lambda t_d}(1-e^{-\lambda t_c}) \times I_\gamma \times \varepsilon_\gamma \quad \text{.....(2.9)}$$

where I_γ is the energy specific gamma-ray intensity and ε_γ is the detector efficiency at the specified gamma-energy.

This equation is used for the cross-section measurements in the present experiment.

2.2 Experimental Set-up of Neutron Activation Analysis (NAA)

2.2.1. Irradiation Facility

For the present experiment monoenergetic fast neutrons were produced by J-25 neutron generator at the INST, AERE, Savar, through $^{3}H(d,n)^{4}He$ reaction using 110 keV deuteron beam with a beam current of 200-300μA. The above reaction [$^{2}H + ^{3}H = [He^{5}]^{*} = ^{4}He + n + 17.6$ MeV] has a positive Q-value of 17.6 MeV. The incident deuteron beam which has been accelerated to an energy of about 150 kV interacts which tritium atom in the target to form compound nucleus $[He^{5}]^{*}$. The compound nucleus is in a highly excited state and immediately de-excites into a helium nucleus and a neutron. The two outgoing particles (neutron and alpha- particle) share between them an amount of energy equal to the Q-value plus the kinetic energy of the incident particle ^{2}H and the target particle ^{3}H. The neutron emitted in the forward direction carries away about 14.7 MeV of energy. The rest of the energy appears as the kinetic energy of the alpha-particles. The alpha-particles are absorbed in the holder but the neutron, being very penetrating, escape into the room.

The generator is a 150 keV horizontal type positive ion accelerator manufactured by AID MEYLAN, France. It was supplied by the IAEA under the technical cooperation program. The following are the general specification of the machine:

Maximum high voltage	: 150 kV
Maximum current	: 2.5 mA
Beam diameter	: 10-30 mm
Power consumption	: 5 kVA
Neutron producing reaction	: D-T reaction
Maximum neutron yield	: 2×10^{11} n/cm^2/sec

The machine is surrounded by 5 ft. thick wall made of specially dense concrete walls which completely shield and control the hazardous radiation. A partial view of J-25 neutron generator is shown in figure 2.2.

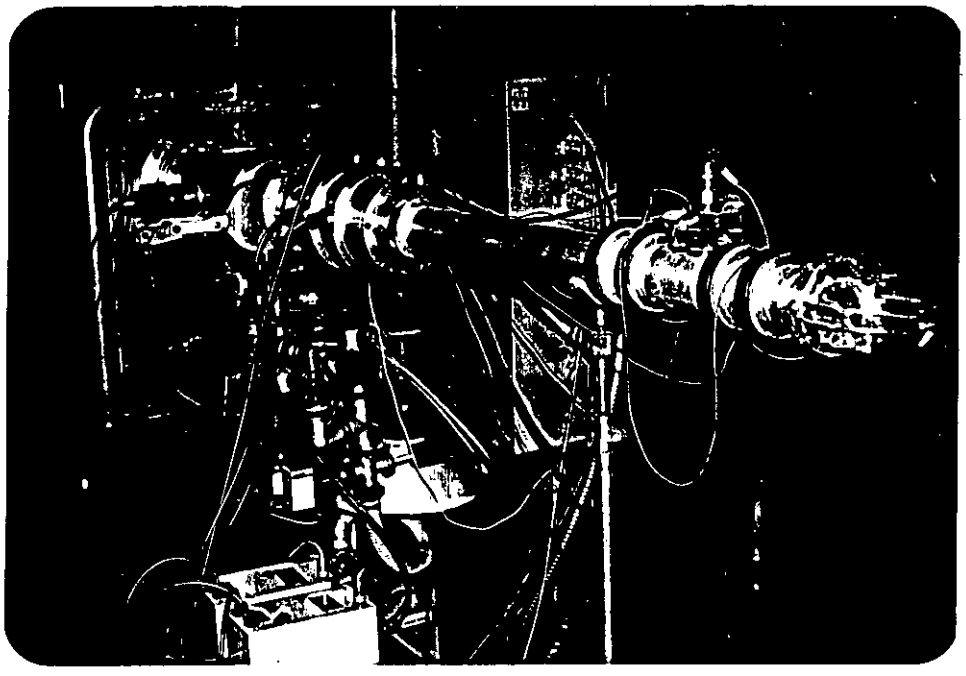

Fig. 2.2. A partial view of J-25 neutron generator.

2.2.2. Gamma-ray Spectrometry System

It is recommended that the spectrometry system be a fully integrated data aquisition and computation system comprising the detector, electronics for pulse amplification and pulse height analysis, and a computer for data processing and analysis.

2.2.2.1. The Detector

Perhaps we should consider the properties of an ideal detector for gamma-ray spectrometry. The requirements which should be less demanding if mere detection rather than spectrometry were the aim, can be summarized as follows: output proportional to gamma-ray energy, good efficiency, i.e., high absorption coefficient, easy mechanism for collecting the detector signal, good energy resolution, good stability, reasonable cost and reasonable size.

First of all it is very desirable that the detector should have a high enough absorption coefficient for gamma radiation so that there is a reasonable probability of complete absorption. In practice the material chosen must provide complete absorption within a detector of available size. This consideration alone rules out gas detectors. Bearing in mind that the absorption coefficients for all the significant interaction processes increase with atomic number we would seek a high atomic number material. Using a solid detection medium rather than a gas significantly decreases the time it takes for the detector to collect the charge carriers created by the deposition of radiation energy in the crystal and also significantly decreases the detector size. This is due to the fact that some solid densities are 1000 times greater than that for a gas [40].

From the above consideration for the utilization of a gamma-ray spectroscopy technique in NAA, semiconductor diode detectors are the best choice. Semiconductor diode detectors use solid semiconductor crystals to which a relatively high voltage is applied. Very high purity levels can be achieved today in a semiconductor crystals by the use of advance technology. This properly allows for greater depletion depths which results in less gamma escapes and subsequently, a greater energy resolution. Detectors made with remarkably high germanium concentrations are referred to as intrinsic germanium, or high purity germanium (HPGe) detectors. In comparison with the Ge(Li) detectors manufactured in the past, they have the advantage of not needing to be cooled when not in use. The germanium crystal is usually cooled by inserting the cryostat in a dewar vessel filled with liquid nitrogen to reduce

the magnitude of the leakage currents to a value that will not affect the detector's energy resolution as shown in fig.2.3.

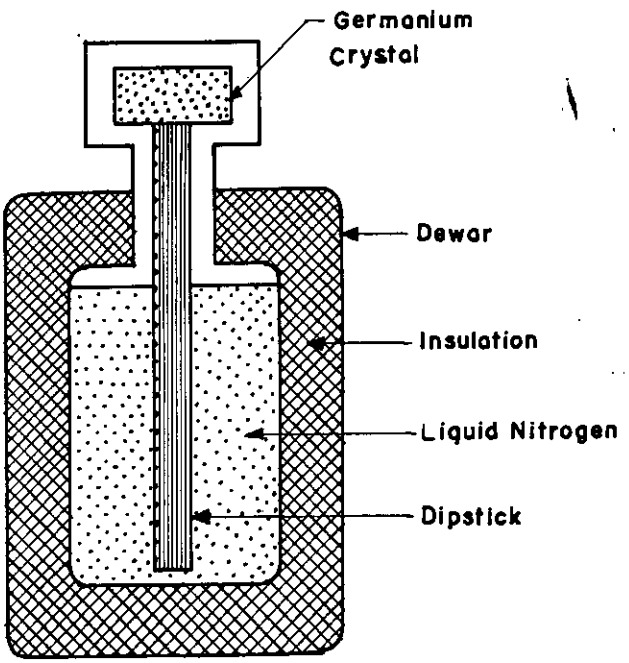

Fig. 2.3. Cross section of a germanium semiconductor diode detector.

There are two types of HPGe detectors, those made of p-type germanium (mainly trivalent elements as residual impurities) and those made of n-type germanium (mainly pentavalent impurities). In figure 2.4 the designations p^+ and n^+ for the contact materials indicate that the materials are highly doped.

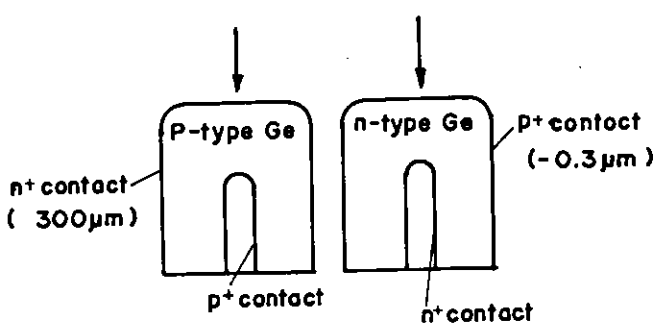

Fig. 2.4. Configurations of closed end coaxial germanium p-type and n-type detectors.

For applications that might involve low energy photons, such as the measurement of ^{241}Am (59.5 keV) or ^{210}Pb (46.5 keV), the use of an n-type detector has considerable advantages over a p type, not only because its peak response is higher, but also because there is less variation in response with energy. This is illustrated in figure 2.5., which shows the typical difference in peak response at low energies for two detectors of the same size.

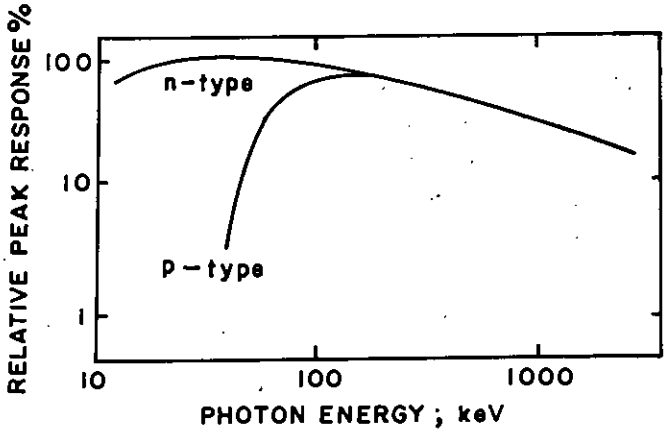

Fig. 2.5. Comparison of typical relative peak response curves for p-type versus n-type germanium detectors.

The most important quantities for characterizing a detector are its relative efficiency, energy resolution, and peak to compton ratio. Efficiency and resolution of HPGe detector are discussed in chapter 3. It is recommended that the peak-to-compton ratio of the detector be greater than 46:1[41]. The peak-to-compton ratio is defined as the ratio of the height of the 1332.51 keV full energy peak in a ^{60}Co spectrum and the height of the flat part of the compton distribution between 1040 keV and 1096 keV as shown in figure 2.6.

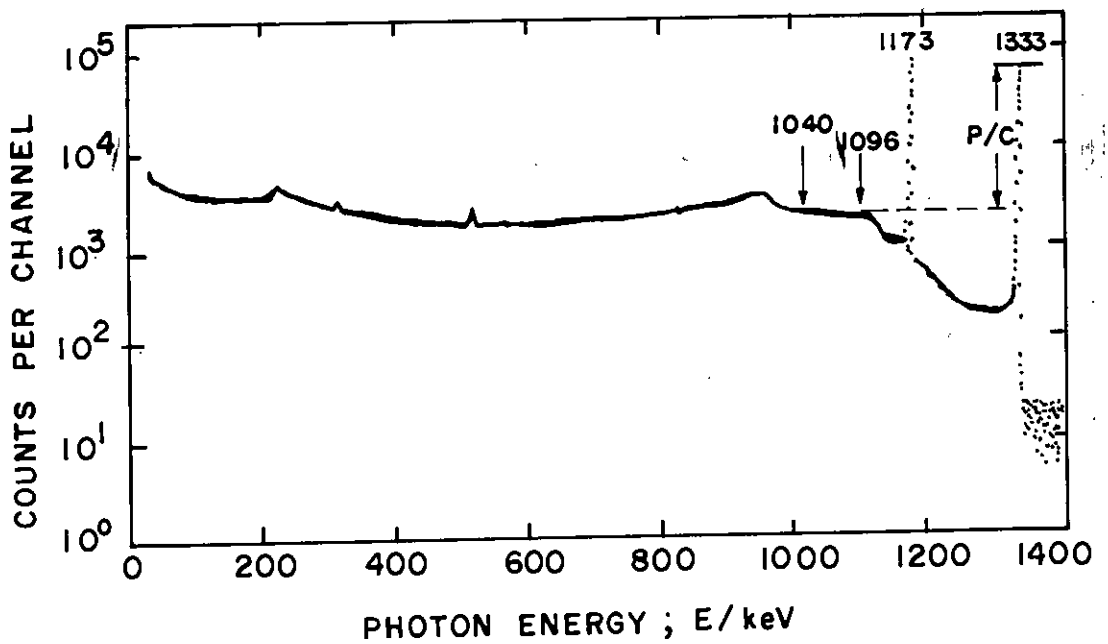

Fig.2.6. Pulse height distribution due to ^{60}Co gamma radiation obtained with a germanium spectrometer. Conventionally the range from 1040 keV to 1096 keV is used as the Compton plateau for the calculation of the peak/compton ratio P/C.

The peak to compton ratio is generally greater the larger the crystal and the better the energy resolution. A large peak to compton ratio is desirable because a low compton background from higher energy lines in the region of lower energy lines facilitates their analysis.

One of the main problems with detectors of this type, however, is that they have a relatively low interaction probability with ionizing radiation compared to NaI(Tl) scintillation detectors. This is an unavoidable trade-off for the high counting efficiency and low resolution characteristics of a germanium detector. It is costly and time consuming to manufacture these large germanium crystals with low impurity concentrations. NaI(Tl) detectors on the other hand, can be produced with larger crystal volumes due to relative ease in manufacturing process compared to HPGe crystals. With the added volume and density,

NaI(Tl) crystal yield a higher interaction probability with radiation and a higher probability for complete absorption of gamma-ray energy. This implies that there are less compton escapes resulting in a larger area underneath the photopeak in question, and thus a higher photofraction compared to germanium detectors.

2.2.2.2. Electronics and Software

The detection of gamma-rays and detailed studies of the spectra were done by a High Purity Germanium (HPGe) detector in conjunction with the associated electronics. A brief description of the associated electronics and software are given below:

- The pre-amplifier is of the charge sensitive type and forms an integral unit with the detector. This device converts charge into voltage pulse and the output pulse is proportional to the energy of the incident photon. This is normally an integral part of the detector unit and is located very near the detector in order to take advantage of the cooling which is necessary for the operation of the detector and which aids the pre-amplifier to operate with low noise. A charge sensitive pre-amplifier model: Canberra no.-2001 is used in the present experiment to get the conversion of charge to voltage pulse.

- A bias high voltage power supply is required to supply high voltage to the detector through the pre-amplifier. The bias voltage across the detector may be from a few hundred volts for a small detector to over 4000V for a large one. The voltage is usually automatically switched off when the detector temperature rises, in order to avoid detector deterioration. The optimum voltage of HPGe detector used in the present experiment is 4000 V and was supplied from the high voltage power supply unit (model: Canberra no.: 3105).

- A spectroscopy amplifier to process the output signals from the preamplifier is required. The important characteristics of the amplifier are the linearity, the output pulse

shape, the gain stability and the noise level. The performance of modern spectroscopy amplifiers is excellent with respect to these characteristics. These amplifiers provide a unipolar output and include pole-zero cancellation and rapid baseline restoration after the occurrence of a pulse. The pulse height network allows the selection of several shaping time constants that determine the pulse width. Longer time constants result in a better resolution, since the system can then average the noise over a longer period of time. On the other hand, the longer time constants lead to more losses and spectrum deterioration due to the pile-up of subsequent pulses at high count rates. As a compromise, a shaping time constant of about 4 μs is frequently chosen. Canberra model-2022 amplifier offers the resolution performance features and flexibility than any other nuclear pulse amplifier that are available commercially and was used in the present experiment.

- A multichannel analyser (MCA) with a minimum of 4096 channels should be connected to a keyboard and display screen for input and output of data and interaction with a computer. Several kits are available for the conversion of computers (PCs) into MCAs. Basically there are three types of conversion kits. One type makes use of a board with analog-to digital converter (ADC) that simply clips into PC; a second type uses a clip-in board with an external ADC; and the third type uses a multichannel buffer (MCB) connected to the PC. All of these PC-based MCA systems are relatively inexpensive and very suitable for use in germanium and NaI gamma-ray spectrometry. In the present gamma-ray spectrometry system, external ADC was used.

- A rapid data acquisition and storage system is needed. For data acquisition in the present experiment, S-100 software which is configured as 4k (4096 channels), 8k (8192 channels), or the entire 16k (16384 channels) was used. The S-100 software allows upto four S-100 MCA boards to operate simultaneously. The S-100 master boards are handling microprocessor bases sub-systems. A typical system configuration is given in fig 2.7. Data storage system consists of magnetic tape, hard disc, floppy disc, or a combination of these media.

- A high speed printer for data output is required. Useful, but not absolutely necessary, is a plotter for archiving spectral drawing.

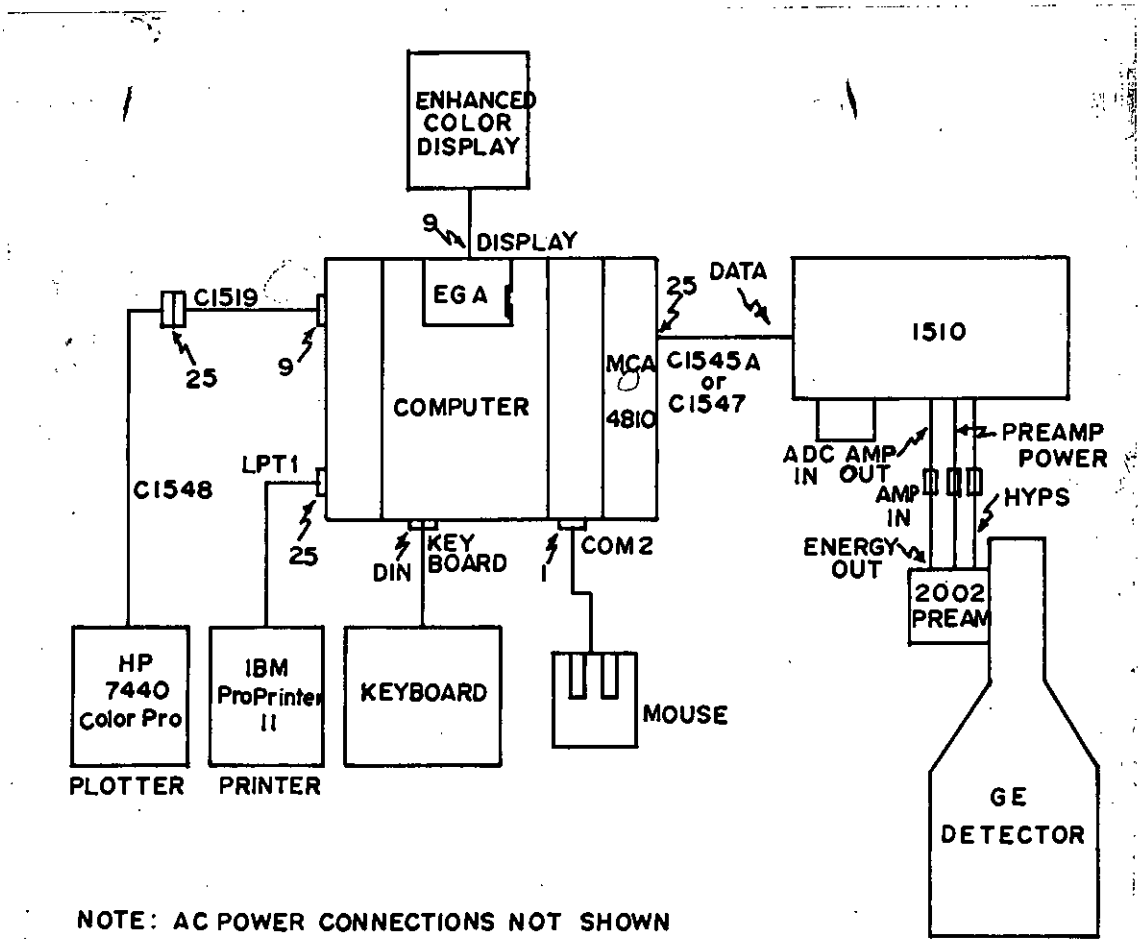

Fig.2.7. Typical system configuration of Gamma-ray spectrometry system.

2.2.2.3. Detector Response

Due to the various types of interaction of gamma radiation with matter, even monoenergetic radiation of energy E leads to a complex detector response. An example is shown in figure 2.6 for ^{60}Co radiation. The measured pulse height distribution

shows the full-energy absorption peak at the high energy end, and towards lower energies a distribution due to partial energy deposition events, consisting of a continuous part and some times, other usually smaller peaks.

Single compton scattering processes in the detector lead to a continuous compton distribution from zero energy to the compton edge at the energy

$$E_c = E\,[\,1 - 1/(1+2E/E_0)] \quad .....(2.10)$$

where E_0 is the electron rest energy (511 keV).

Interaction in the crystal by electron positron pair production results in the single escape peak at $E-E_o$, the double escape peak at $E-2E_o$, and also a continuum due to partial energy deposition following compton scattering of annihilation photons as illustrated in figure 2.8. The escape of bremsstrahlung and of fluorescence radiation also has an effect on the shape of the observed spectrum.

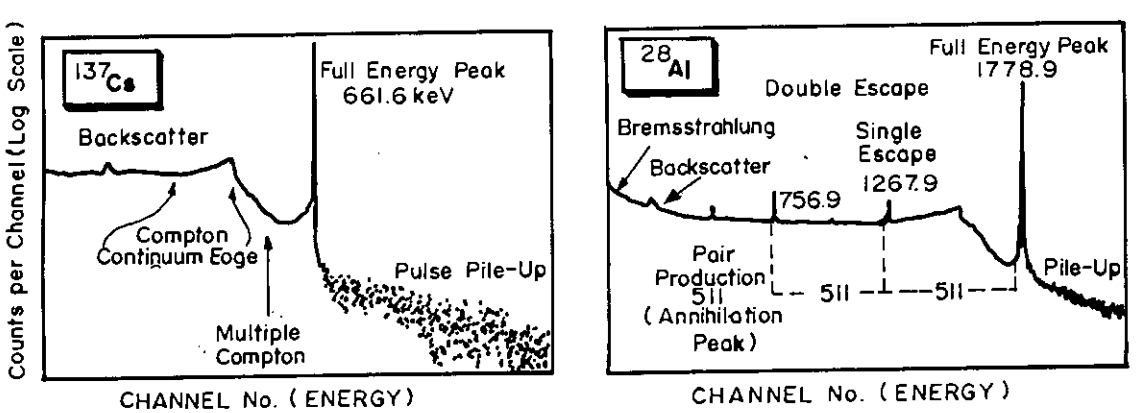

Fig. 2.8. Example spectra illustrating the various features spectral expected.

Compton scattering in the non-active parts of the detector, e.g., in the detector mounting materials or in the cryostat, leads to scattered photons which can also be detected.

The resulting scattering distribution in the pulse height spectrum usually exhibits a broad backscatter maximum at an energy E/[1+(2E/Eo)].

Pair production in surrounding materials leads to a peak at 511 keV and photoelectric absorption to fluorescence radiation peaks. Even electrons produced outside the effective detector volume can contribute directly or via bremsstrahlung to the recorded spectrum.

2.2.2.4. Peak Position and Area

The basic task of gamma-ray analysis program is to find and identify the peaks and to deduce the peak area.

When there are many peaks to be located in a spectrum, automatic peak search routines are of particular value. The peak search procedure does not need to initiate if specific radionuclides are expected. In this case a manual setting of windows in the corresponding energy region is preferable.

The peak position can usually be determined with an uncertainty of less than a tenth of a channel. For 4096 channels and a total energy range of 2 MeV, this means that the energy can be obtained with an uncertainty of the order of 0.1 keV. If a particular radionuclide is expected, the corresponding region of interest can be set in advance, and the determination of the peak position becomes unnecessary.

Somewhat more problematical is the determination of the number of counts in the peak (peak area). The simplest method is the summing of all counts in the channels containing the peak and subtracting the background from these total counts. A typical gamma-ray spectrum is illustrated as in figure 2.9.

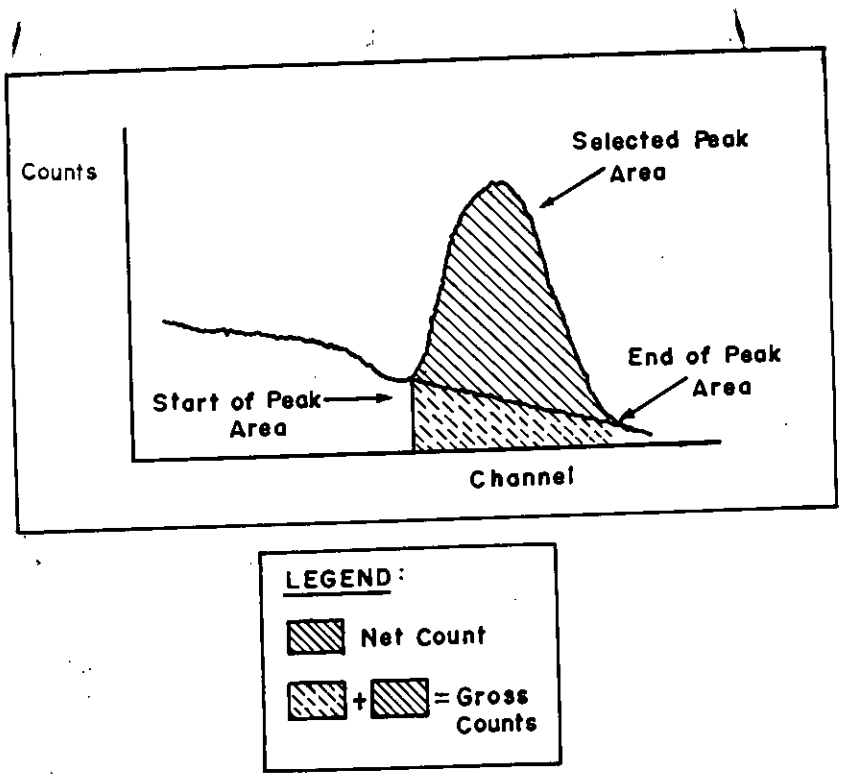

Fig. 2.9. A typical gamma-ray spectrum of a photo peak.

CHAPTER-3

STUDY OF DETECTOR PARAMETERS

STUDY OF DETECTOR PARAMETERS

The most important parameters characterizing a detector are efficiency, energy resolution, chi-square test, etc. All of these parameters are the function of gamma-ray energy. The better performance of the detector depends on the higher resolving power and the higher value of efficiency. The stability of the detector depends on the chi-square value of a particular gamma-ray energy. High purity germanium (HPGe) detector have been used in the present experiment and the above mentioned parameters have been studied to control the quality and stability of the detector.

3.1. Chi-square Test of HPGe Detection System

One of the important parameters of the counting equipment in the INAA is the stability. The instability of apparatus becomes significant for long counting times due to gain changing and spectrum shifting. A typical theoretical temperature instability of 0.0075%/K means that a 1° change in temperature may shift a peak in channel number 4096 by 0.3 of a channel [42]. Corrosion and dust in the spectrometer parts such as the main amplifier and the high voltage supply cannot always be avoided. Instability of the spectrometer leads to a spectrum shift during counting time and in consequence to worse resolution (FWHM) of the peaks. As such it is essential to perform stability test of the detection system every time before counting.

Chi-square test have been performed for HPGe detection system used in the present experiment. This test is based on 10 separate counts each of which have been counted for the same period long enough to accumulate at least 10,000 counts for each count period. For stability, chi-square must lie between 3.35 and 16.92[43].

For testing low and high energy stability 122.02 keV (emitted from point source ^{57}Co) and 1332.51 keV (emitted from point source ^{60}Co) gamma ray energies were used. ^{57}Co and ^{60}Co point sources were counted individually for 1000 sec and 500 sec respectively. Gamma-ray counts under 122.06 keV and 1332.51 keV peaks were recorded and shown in table 3.1.

Table-3.1: Gamma-ray counts for chi-square test

No.of Counts	γ-ray emitted from ^{57}Co Source	γ-ray emitted from ^{60}Co Source	
	122 keV	1173.23 keV	1332.51 keV
Counts 1	13680	14682	13350
Counts 2	13501	14370	13244
Counts 3	13472	14506	13053
Counts 4	13699	14566	13092
Counts 5	13557	14243	13218
Counts 6	13529	14602	13111
Counts 7	13273	14330	13096
Counts 8	13613	14369	13063
Counts 9	13432	14493	13128
Counts 10	13734	14381	12945
X^2	1835930554	2089409140	1724085748
X	135490	144542	131300
Chi-square	13.03	11.79	8.87

The familiar equation for chi-square test is given below:

$$\chi^2 = \frac{[X^2 - \{(X)^2 / 10\}]}{\overline{X}}$$

where, X^2= sum of the squares of 10 readings

X = sum of ten readings

$\overline{X}$ = mean value of ten readings

Using this equation and data from table 3.1 chi-square obtained are 13.03, 11.79 and 8.87 for 122.06 keV, 1173.23 keV and 1332.51 keV gamma-ray energies respectively.

From these results we concluded that the HPGe counting system used in the present experiment is stable and the results produced using the system is reliable.

3.2. Energy Resolution of HPGe Detector

Energy resolution is one of the important parameter of a detector. The resolving power or resolution of a detector is defined as the ability of the detector to separate two closely spaced peaks in a gamma-ray spectrum. The resolution of the detector is affected by the counting rate and by amplifier settings other than the time constant. So detector resolution is usually specified at low counting rate.

The resolution of the HPGe detector is measured using ^{60}Co point source and a spectrum is accumulated by placing the source on the detector which was properly shielded by lead and iron to minimize the background radiation. The output of the detector was collected in a personal computer based multichannel analyser with the help of S-100 software through a pre-amplifier, amplifier and an ADC (Analog to Digital Converter).

^{60}Co isotopes emits two cascades gamma-rays at the energies 1173.23 and 1332.51 keV. The experimental data from the spectrum is plotted by putting channel number in X-axis and counts in Y-axis and the spectrum is shown in fig.3.1.

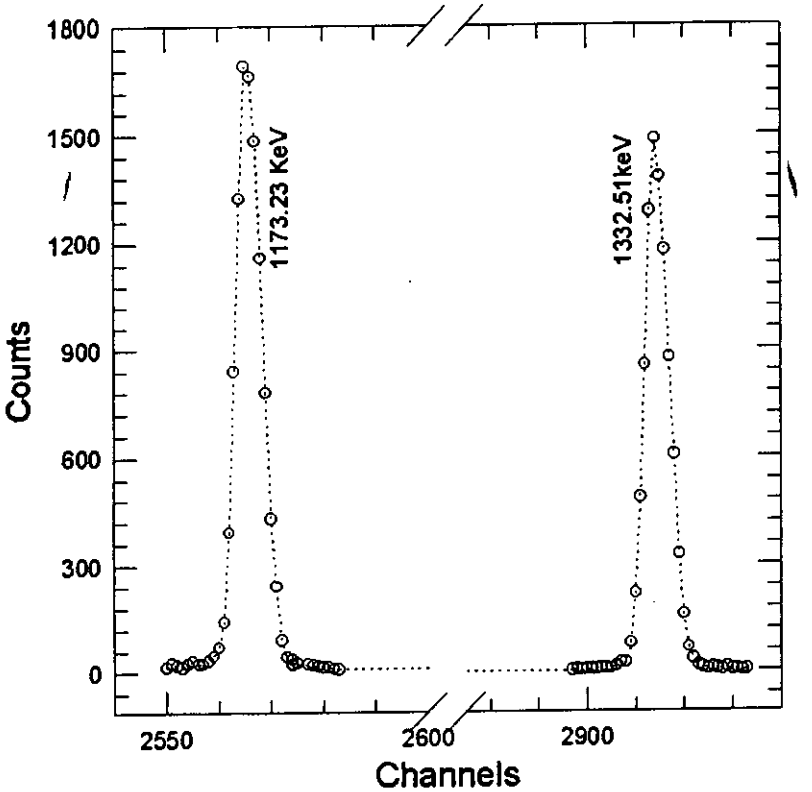

Fig. 3.1. Gamma-ray spectrum for the measurement of Energy resolution of HPGe Detector.

The full width at half maxima (FWHM) is determined from the graph and is found to be 5.83 channels at 1332.51 keV peak. The resolution is given by the following equation.

$$\text{Resolution} = \text{FWHM(in channel)} \times \frac{\text{Difference of the gamma-ray energy peak}}{\text{No. of channel between two peaks}}$$

$$= \text{FWHM} \times \frac{E_2 - E_1}{C_2 - C_1}$$

$$= 5.83 \times \frac{1332.51 - 1173.23}{2914 - 2565}$$

$$= 2.66 \text{ keV}.$$

The resolution is obtained to be 2.66 keV at 1332.51 keV gamma line of ^{60}Co point source. The lower value indicates the good resolution of the detector.

3.3. Energy Calibration of HPGe Detector

The objective of energy calibration is to derive a relationship between peak position in the spectrum and the corresponding gamma-ray energy. This is normally performed before measurements, if only in a preliminary manner, but it is usual for spectrum analysis programs to include more sophisticated calibration options within the subsequent data reduction.

Energy calibration is accomplished by measuring the spectrum of a source emitting gamma-rays of precisely known energy and comparing the measured peak position with energy. It matters not whether the source contains a single nuclide or several nuclides. In the present experiment ^{152}Eu point source was used for energy calibration. Whatever source is used it is wise to ensure that the calibration energies cover the entire range over which the spectrometer is to be used.

In practice it is sufficient to measure the spectrum long enough to achieve good statistical precision for the peaks to be used for the calibration. The calibration process then involves marking the peaks to be used and their true energy. The computer can then search for the peaks, measure the peak position to a fraction of a channel and reduce the energy/channel relationship. Figure 3.2. shows an energy calibration using ^{152}Eu point source. Ten points are plotted together with the best fit straight line. Normally the spectrometer from which the data of figure 3.2 were obtained would be calibrated using only the two points marked. The data shown appears to fit a linear relationship very well; it cannot take into account any integral non-linearity in the system.

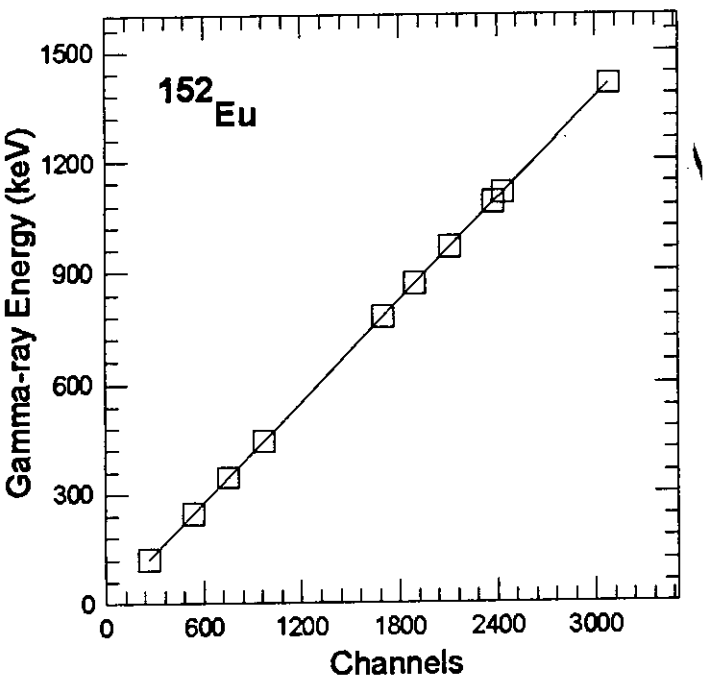

Fig.3.2. Energy calibration using ^{152}Eu source (Ten points and the best fit straight line)

The most appropriate relationship to fit the data are given below:

$$E\ (keV) = I + GC$$

where I and G are the intercept and gradient of the calibration line and C the channel position. In several years of general gamma-spectrometry many authors have found no need for other than a two point energy calibration[40].

3.4. Efficiency Calibration of HPGe Detector

The efficiency calibration of a HPGe detector should be known before use. The efficiency of a detector is the proportionality constant that relates the activity of the source being counted and the number of counts observed. By knowing the efficiency of a detector,

the true activity of sources can then be calculated. The following discussions are referred to the different kinds of efficiency definitions that are in common use for gamma-ray detectors:

Relative efficiency is a general performance measure relating the efficiency of detection of the ^{60}Co gamma-ray at 1332.51 keV of the HPGe detector to that of a standard NaI(Tl) scintillation detector.

In gamma spectrometry our intention is to relate the peak area in our spectrum to the amount of radioactivity it presents. For this we need the ***absolute efficiency***. This relates the peak area to the number of gamma-rays emitted by the source and must depend upon the geometrical arrangement of source and detector.

Absolute total efficiency relates the number of gamma-rays emitted by the source to the number of counts detected anywhere in the spectrum. This takes into accounts the full energy peak and all incomplete absorptions represented by the compton continuum.

Intrinsic efficiency (full-energy peak or total) relates the counts in the spectrum to the number of gamma-rays incident to the detector. This efficiency is a basic parameter of the detector and is independent of the source/detector geometry.

Full energy peak is the most significant parameter in practical gamma spectrometry. In the present work only the intrinsic ***full energy photo peak efficiency*** is calculated. The calculation of full-energy peak efficiency is straight forward; it is the ratio of the number of counts detected in a peak to the number emitted by the source.

$$\text{Efficiency } (\varepsilon) = R / (S \times I_\gamma) \text{ ------- } (3.1)$$

R is the full-energy peak count rate in counts per second. S is the source strength in disintegration per second (i.e., bacquerels) and I_γ is the probability of emission of the particular gamma-ray being measured.

The source strength used in eqn. (3.1) need to be corrected for decay from the date of preparation i.e, the present activity is given by:

$$S_t = S_o e^{-\lambda t} \quad \text{----------} \quad (3.2)$$

where S_o and S_t are the original and present source strength (activities) respectively, t is the decay time, λ is the decay constant = $\ln 2/T_{1/2} = 0.693/T_{1/2}$, where $T_{1/2}$ is the half-life of the source. Thus

$$\text{Efficiency (\%)} = [R / (S \times I_\gamma)] \times 100 \quad \text{--------} \quad (3.3)$$

The known strength standard radioactive point sources of ^{22}Na, ^{54}Mn, ^{57}Co, ^{60}Co ^{133}Ba, and ^{137}Cs gamma-rays of different energies were used for the measurements of detector efficiency. These sources are chosen in such a way that it covers a region of interest with maximum number of points in between. The gamma-ray emitted from the sources are in range of 80.99 keV to 1332.51 keV. The sources were placed individually at the mid point of the surface of the detector. The output signal of the detector was obtained via preamplifier, amplifier and ADC to the PC based MCA. From the accumulated spectra the net area under a photo peak is determined and then by using the source strength and gamma-ray intensity, the efficiency of the HPGe detector were measured.

The standard sources used for the efficiency measurement emit more than one gamma-rays. As such there is a certain probability of missing counts under the photo peak by coincidence loss of cascade gamma-rays when the source remain closer to the detector[44]. Coincidence loss may be eliminated by taking counts of the sources at distant point from the detector[27]. In order to correct the coincidence loss effects for two cascade gamma-rays, the activity ratio of ^{60}Co to the monoenergetic gamma-ray source of ^{137}Cs were measured as the function of the distance between the source and the detector. The ratio is plotted in fig. 3.3.

The ratio at the 12 cm source to detector distance is 1.0 i.e., there is no coincidence loss for distances greater than this.

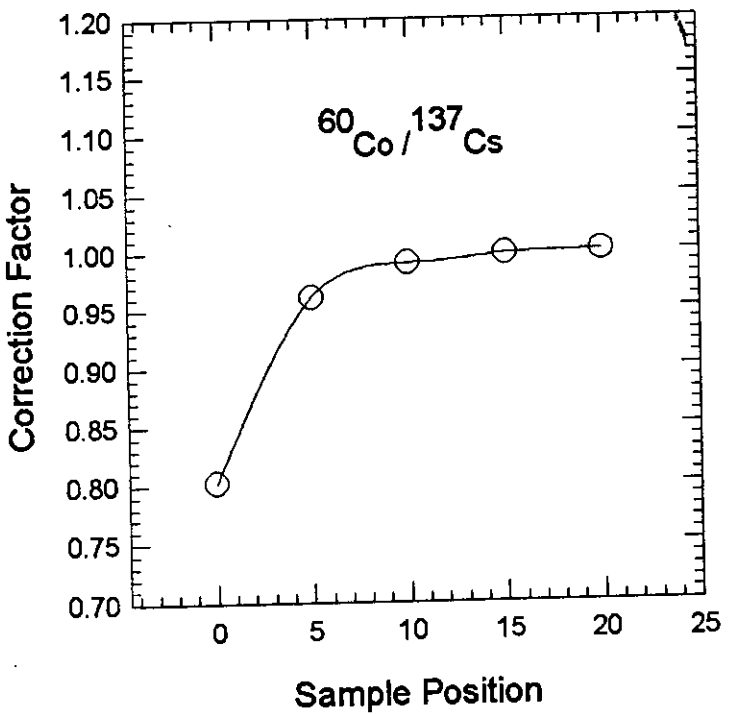

Fig. 3.3. Correction factor of the sum peak for a HPGe detector.

Thus, the efficiency of the thirteen gamma energy points using the standard sources determined at 12 cm above the detector is used to determine the efficiency at the surface of the detector. Since ^{137}Cs and ^{54}Mn has single gamma-line and do not suffer any coincidence loss, these sources are used to determine the efficiencies of cascade gamma-rays at the surface of the HPGe detector. Taking the efficiency ratios of 834.81 keV gamma-ray (from ^{54}Mn) at surface and at 12 cm above the detector, the other efficiencies are normalized at the surface of the detector. Same procedure was applied for another single line gamma-ray energy 661.64 keV (from ^{137}Cs). The normalizing factors given from 834.81 keV and 661.64 keV are nearly same. Finally the average efficiency for each energy peak is taken which are generated by normalizing with the 834.81 keV and 661.64 keV gamma-lines. The experimental data is given in table 3.2. The data for efficiency using normalizing factors is given in table 3.3. A graph is plotted with energy along X-axis and normalized average

surface efficiency along Y-axis which is illustrated as in figure 3.4.

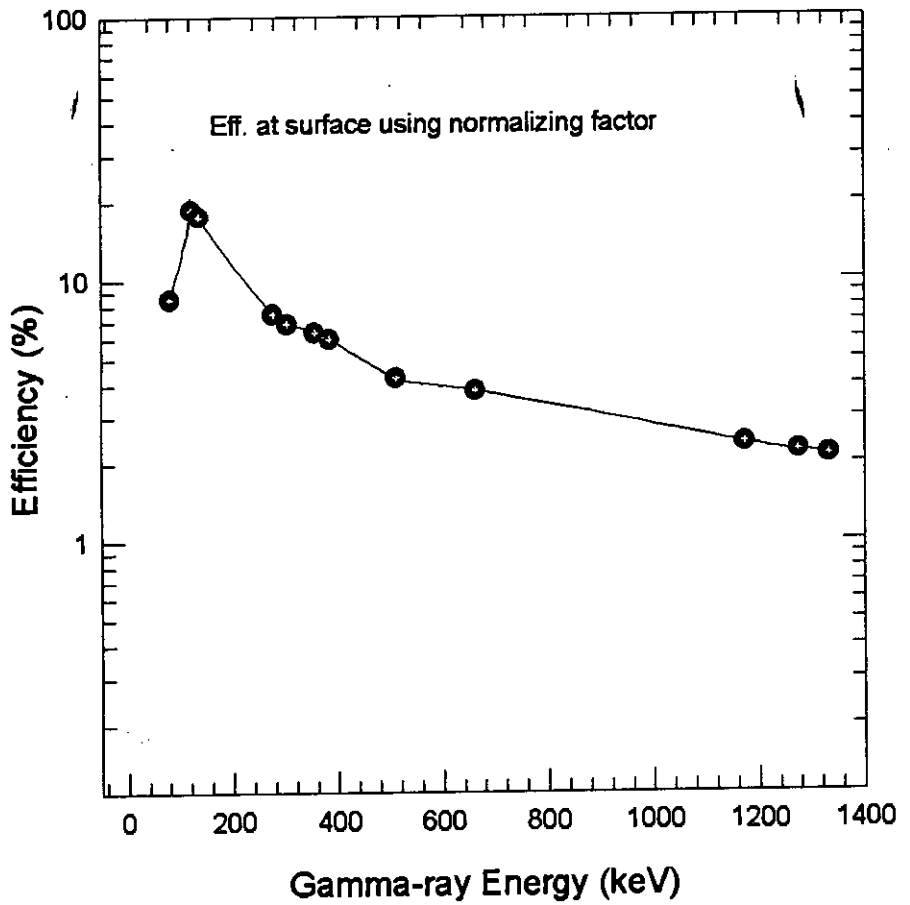

Fig. 3.4. Efficiency curve for HPGe detector

The low efficiencies observed at low energies is due to photon absorption by sample matrix, cryostat endcap and the dead layer in the detector. The maximum efficiency obtained at 122 keV is due to the compton absorption. The gradual decrease of efficiency at high energies occurs because of the reduction in the interaction cross-section of the high energy photons.

Table 3.2. Efficiency calibration data at 12 cm above the HPGe detector surface.

Point source	Initial strength (S_0)	Half-life $T_{1/2}$	Present activity $S_t=S_0e^{-\lambda t}$	γ-ray energy (keV)	γ-ray intensity I_γ (%)	Count per sec. (CPS)	Efficiency ε (%)
^{60}Co	37259	5.272 y	19351	1173.23 1332.51	99.88 100.00	43.86 39.40	0.227 0.204
^{57}Co	42550	271.3 d	354	122.06 136.48	85.51 10.61	5.4 0.633	1.784 1.685
^{54}Mn	40959	312.2 d	640	834.81	99.98	2.323	0.375
^{137}Cs	33411	30.17 y	30376	661.64	86.00	94.808	0.363
^{22}Na	41551	2.66 y	11084	511.00 1274.55	181.08 99.94	81.371 23.510	0.405 0.212
^{133}Ba	34965	10.5 y	25458	80.99 276.40 302.85 356.01 383.85	35.40 7.30 18.40 61.91 8.91	73.001 13.181 30.521 95.321 12.965	0.810 0.709 0.652 0.605 0.572

Table 3.3. Efficiency at the surface of HPGe detector using normalizing factor.

$$Normalizing\ factor\ for\ Cs = \frac{Efficiency\ at\ the\ surface\ of\ the\ detector}{Efficiency\ at\ 12\ cm\ above\ the\ detector\ surface} = \frac{0.0377}{0.00363} = 10.5141 \quad and$$

$$Normalizing\ factor\ for\ Mn = \frac{Efficiency\ at\ the\ surface\ of\ the\ detector}{Efficiency\ at\ 12\ cm\ above\ the\ detector\ surface} = \frac{0.0394}{0.00375} = 10.3859$$

γ-ray energy (keV)	Eff. (%) using normalizing factor for ^{137}Cs	Eff. (%) using normalizing factor for ^{54}Mn	Average Efficiency ε (%)
80.99	8.413	8.516	8.465
122.06	18.528	18.757	18.640
136.48	17.500	17.716	17.608
276.40	7.364	7.454	7.409
302.85	6.772	6.855	6.814
356.01	6.283	6.361	6.322
383.85	5.941	6.014	5.978
511.00	4.206	4.258	4.232
661.64	3.770	3.817	3.794
834.81	3.895	3.943	3.919
1173.23	2.358	2.387	2.373
1274.55	2.202	2.229	2.216
1332.51	2.119	2.145	2.132

CHAPTER-4

EXCITATION FUNCTION MEASUREMENTS OF $^{63}Cu(n,\alpha)^{60}Co$ REACTION IN THE NEUTRON ENERGY RANGE 13.82-14.71 MeV

Excitation Function Measurements of $^{63}Cu(n,\alpha)^{60}Co$ reaction in the Neutron Energy Range 13.82-14.71 MeV

4.1 Introduction

Measurements of activation cross sections for production of long-lived radionuclides at around 14 MeV neutron energy are of interest for testing nuclear reaction models, determining the waste disposal and recycling aspects of fusion reactor materials. Furthermore, the data in the case of structural materials of a fusion reactor are important for the estimation of neutron multiplication, nuclear heating, nuclear transmutation and radiation damage effects. Cross section data available for reactions leading to product nuclei of long half-life are often contradictory around 14 MeV especially in the case of $^{63}Cu(n,\alpha)^{60}Co$ reaction. This is due to low fluxes of monoenergetic neutrons available by accelerators which induce only very low activities. Cross section data of (n,α) reaction are of considerable interest in fusion reactor technology for estimating helium production in potential constituents of first wall and structural materials.

Copper is a significant material of magnetic coil for fusion reactor[17]. Therefore the cross sections of $^{63}Cu(n,\alpha)^{60}Co$ reaction are very interesting for understanding irradiation damage and the material performance under exposure to intense neutron flux. Since ^{60}Co has a long half-life of 5.27 years, the activity of ^{60}Co is also an important factor for waste treatment and maintenance of the facility.

Many experimental and theoretical evaluation works[15-23, 45-49] were carried out for the measurement of activation cross sections of $^{63}Cu(n,\alpha)^{60}Co$ reaction. But there are still some unexplained discrepancies among the existing experimental data in the literature. The present work aims at removing the existing discrepancies in the literature data by providing precise and accurate data along with some newer points in between for the first time. Using

the activation technique in combination with the high resolution gamma-ray spectroscopy, high precision measurements were carried out for the reaction of $^{63}Cu(n,\alpha)^{60}Co$ in the neutron energy range from 13.82 MeV to 14.71 MeV.

A computer code SINCROSS-II[36] - a nuclear cross section calculation system with simplified input format were used for the theoretical estimation of activation cross section. The measured cross section values were compared with the recent literature data.

4.2. Experimental Procedures

For the measurement of activation cross section of $^{63}Cu(n,\alpha)^{60}Co$ reaction in the neutron energy range from 13.82 MeV to 14.71 MeV, the following prominent characteristics are involved.

4.2.1. Neutron Source

The experiment was performed at fast neutron source, J-25 neutron generator facility of the Institute of Nuclear Science & Technology (INST), Savar, Dhaka. D-T neutrons were produced by bombarding a air cooled, 3.7×10^{11} Bq copper backing tritium target with a 110 keV deuteron beam (d^+). The diameter of the tritium target (1mm thick copper backing) is 4.9 cm with a active layer diameter 2.5 cm. The target assembly was designed in order to reduce neutron scattering by the assembly itself as possible. The maximum neutron yield is about 2×10^{11} n/cm^2/sec.

4.2.2. Samples

Since four cross section values of $^{63}Cu(n,\alpha)^{60}Co$ reaction have been measured with respect to four neutron energies and since the neutron energy depends on the angle of emission, four copper samples were prepared using high purity (≥99.99%) metallic copper foils of isotopic composition with the dimension of 1cm×1cm×1mm. Niobium foils of the same size as the sample were then attached in front and at the back of each copper sample. Niobium foils were used to measure the neutron flux at the sample position. Samples varied from 1.51659gm to 1.69147gm and that of niobium foils from 0.16654gm to 0.25435gm.

4.2.3. Irradiation

The prepared copper samples sandwiched with Nb foils were irradiated at 0°, 40°, 80°, and 120° (corresponding to neutron energies of 14.71 MeV, 14.57 MeV, 14.21 MeV, and 13.82 MeV) with respect to the deuteron (d^+) beam direction in a ring geometry arrangements as in figure 4.1 over a period of 11.60 hours with a 300 μA beam current in such a way that they are equidistant from the center of the beam. The distance between the beam spot and the sample

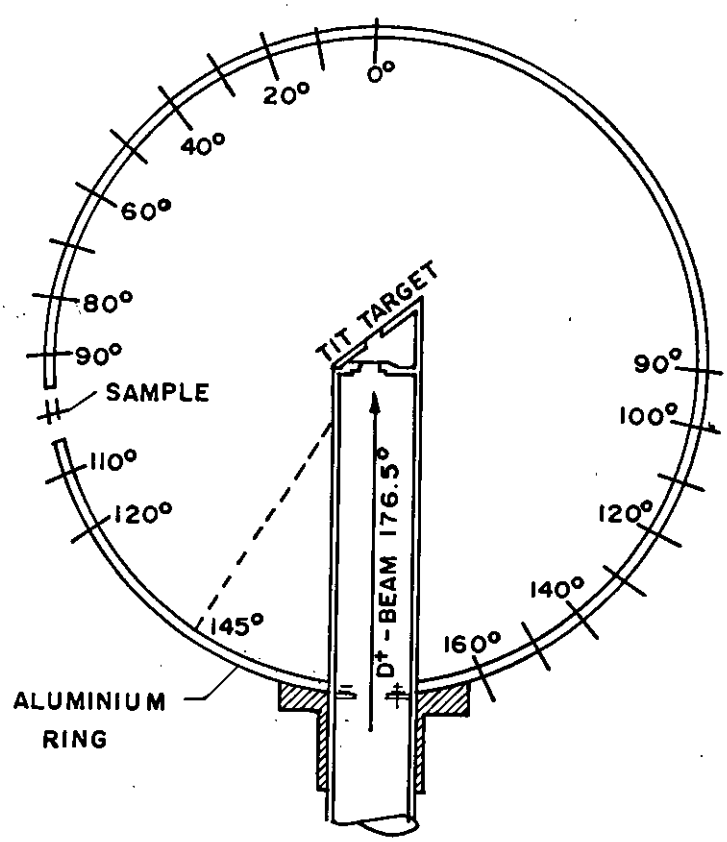

Fig. 4.1. Ring geometry arrangement of J-25 Neutron Generator (AID, France).

center was 6 cm. The effective neutron energies corresponding to the emission angle were verified by measuring the ratio of ^{89}Zr to ^{92m}Nb specific activities induced both in Zr and Nb

foils by (n,2n) reactions[11]. The neutron production in time was monitored by means of a BF_3 long counter calibrated earlier with a 20 μg ^{252}Cf neutron source.

4.2.4. Neutron Flux Monitor

After irradiation the neutron flux densities effective at each sample position in the irradiation with D-T neutrons were determined via the monitor reaction $^{93}Nb(n,2n)^{92m}Nb$; $T_{1/2}$=10.14 days, E_γ =934.51 keV, I_γ =99.2%. The value 464 mb (±4.2%) was adopted as the standard cross section of $^{93}Nb(n,2n)^{92m}Nb$ reaction for neutron energies from 13.82-14.71 MeV[27]. The $^{93}Nb(n,2n)^{92m}Nb$ dosimetry reaction was adopted as the neutron flux monitor because the cross section is relatively large around 14 MeV and the half-life of ^{92m}Nb is of convenient length (10.14 days). For the four irradiation angles used, the neutron flux densities were of range between 0.7531×10^6 and 1.2018×10^6 n/cm^2/sec.

4.2.5. Gamma-ray Measurement

The decay scheme of reaction product ^{60}Co are shown in figure 4.2.

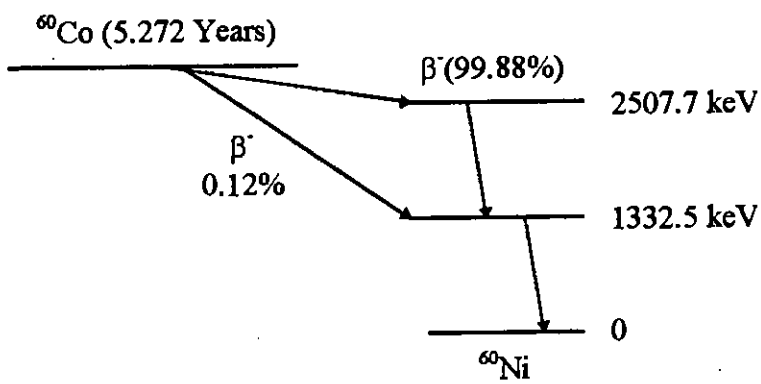

Fig. 4.2. Decay scheme of ^{60}Co

Many gamma transitions are involved in the decay scheme of ^{60}Co, where the great majority of beta decays go to the 2505.7 keV level which falls to the ground state in two steps. Thus two gamma-rays appear:

$$\gamma_1 = (2505.7 - 1332.5) = 1173.2 \text{ keV}$$

$$\gamma_2 = (1332.5 - 0) = 1332.5 \text{ keV}$$

Two gammas are said to be in cascade.

After irradiation, the intensity of the 1173.2 keV and 1332.51 keV gamma-lines emitted from the product nucleus of $^{63}Cu(n,\alpha)^{60}Co$ reaction was measured for each sample using High Purity Germanium (HPGe) detector. The gamma-ray spectra were accumulated and analysed in Multi Channel Analyser (MCA) based IBM PC-AT computer using the software S-100 coupled with associated electronics (pre-amplifier, amplifier, analog to digital converter, high voltage unit, etc.). The detector was shielded with lead and iron to reduce the background radiation. During each measurement, the natural background counts were periodically checked and subtracted from the total counts to obtain the real counts of the investigated gamma-line of the same gamma-ray.

Since ^{60}Co has a long half-life (5.27 yrs) and the low activity produced in the product nuclei, each sample was counted over a long period (counting time varied from 2.75×10^5 sec - 3.0×10^5 sec). The measured counts under the photo peak were subjected to usual correction for dead time loss, pile up loss and coincidence effect.

4.2.6. Cross Section Calculation and Error Estimation

The count rate of gamma-ray emitters, corrected for background effects, were used to calculate the cross sections using the well-known activation formula deduced in chapter-2, equation number 2.9. The major sources of errors and their magnitudes are given in table 5.4. The total error of each cross section value was obtained by taking the square root of the sum of squares of the individual errors in quadrature. The overall uncertainties for the present work were in the range of 5-10%. The largest errors in cross sections of reaction determined via gamma-ray spectrometry originated from the poor counting statistics.

In order to describe the measured excitation functions, nuclear model calculations were performed using the computer code SINCROSS-II.

4.3. Results and Discussion

Cross sections were determined from photo peak counts by using nuclear decay data e.g. half-life, gamma-ray energy, gamma intensity, isotopic abundance, etc. were taken from Lederer [50] shown in table 4.1. For each run the cross section was determined by averaging the values obtained by using the photo peak counts for both the 1173.23 keV and 1332.51 keV gamma-rays resulting from ^{60}Co.

The measured cross sections including errors and the neutron flux obtained from the present experiment for $^{63}Cu(n,\alpha)^{60}Co$ reaction in the neutron energy range 13.82-14.71 MeV are given in table 4.2. The quoted uncertainty in cross section values includes both statistical and systematic errors. The estimated uncertainty in the cross section values lies between 5 to 10%. Considering the long half-life and complex decay scheme of ^{60}Co, the

uncertainty is satisfactory. The principal sources of the systematic errors along with their magnitudes considered are shown in table 5.4.

The cross section obtained in the present measurements together with the recent literature values are plotted as a function of neutron energy shown in figure 4.3.

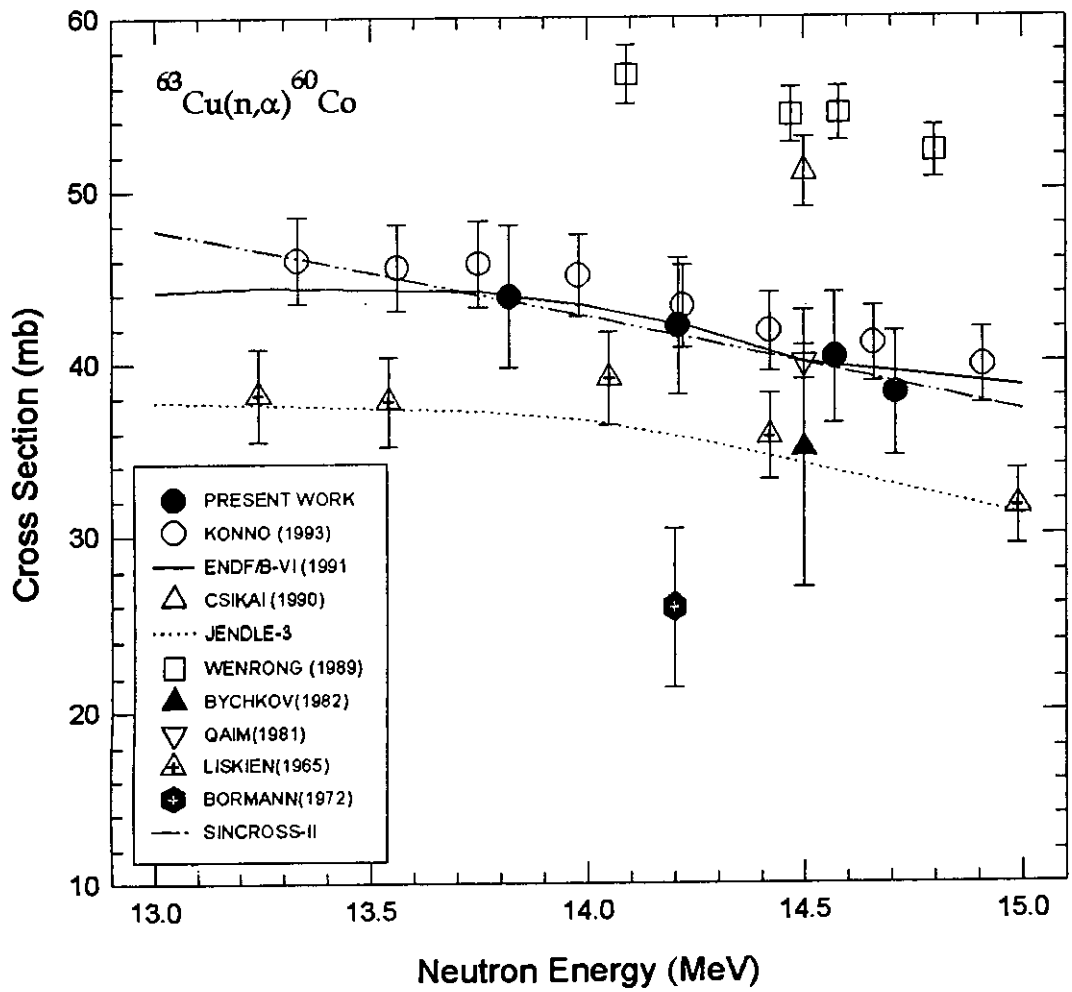

Fig. 4.3. Excitation Function of $^{63}Cu(n,\alpha)^{60}Co$ Reaction.

Compared to the present results, the measurements due to Zhao Wenrong, et.al.[17], and J. Csikai et. al.[18] show faster rise in the cross section from 14.09 to 14.80 MeV. The

present results agree well with experimental and evaluated data recently reported by Chikara Konno[16] and ENDF/B-VI[21]. On the other hand, JENDLE-3[22] (which is based on the experimental data of Paulsen[15]), Bormann[23] , Bychkov et. al.[20] appears to give a value lower than the value obtained in the present work. Therefore, it is necessary to re-evaluate this reaction for JENDLE-3. It is also Worth mentioning that the present experimental data given in figure 4.3. agree with the results obtained using computer code SINCROSS-II[36]. The (n,α) excitation function for $^{63}Cu(n,\alpha)^{60}Co$ reaction is thus well established.

Table 4.1. Decay data of nuclear reaction product ^{60}Co [50].

Nuclear reaction	Isotopic abundance (%)	Q-value (MeV)	Half-life of the product nuclei (Year)	Gamma-ray energy (keV)	Gamma-ray intensity (%)
$^{63}Cu(n,\alpha)^{60}C0$	69.2	1.656	5.27	1173.21	100.00
				1332.51	99.98

Table 4.2. Measured cross sections with neutron flux.

Emission Angle	Corresponding Neutron Energy (MeV)	Neutron Flux ($n.cm^{-2}.sec^{-1}$) $\times 10^6$	Measured Cross Sections (mb)
0°	14.71 ± 0.115	1.2018	38.20 ± 3.21
40°	14.57 ± 0.108	0.9940	40.25 ± 3.65
80°	14.21 ± 0.060	0.8939	42.13 ± 4.01
120°	13.82 ± 0.060	0.7531	43.87 ± 4.30

CHAPTER-5

EXCITATION FUNCTIONS OF (n,2n) PROCESSES ON SOME ISOTOPES OF Cl, Mo, AND Ce IN THE ENERGY RANGE 13.90 - 14.71 MeV

Excitation Functions of (n,2n) Processes on Some Isotopes of Cl, Mo, and Ce in the Energy Range 13.90 - 14.71 MeV

5.1. Introduction

Neutron activation cross section data around 14 MeV have become important from the view point of fusion reactor technology. Fusion energy is a very important, inexhaustible energy source for future generations of mankind. The most promising near-term fusion fuel cycle is the deuterium-tritium (D-T) cycle because of its large reaction cross sections at relatively lower plasma temperature. Interaction of neutrons with engineering components such as blanket and shield, which surround the fusion reacting plasma, is an important process as far as energy extraction and radiation shielding are concerned. Adequate knowledge of the activation cross section is necessary for the design of these engineering components, the assessment of their nuclear performance, and radiological characteristics[51]. They also provide the response functions required for neutron dosimetry of fusion environment. Finally, they are useful to confirm predictions of nuclear reaction theory.

At present, there is a bulk of experimental data on nuclear cross sections in the 14 MeV energy region. However, it is quite a typical situation, especially in the case of (n,2n) reaction on chlorine[7,8,24-28], molybdenum[9,10,24,27,29-32] and cerium[17,19,20,28,33-34] isotopes, where the data scattering exceeds the errors cited by authors. This often excludes a possibility to obtain an evaluation of high accuracy. To a large extent, this situation is, probably, due to the fragmentary character of many experiments. It is a difficult problem to select preferable data as a main source to estimate the quantity.

Chlorine, molybdenum, and cerium are the components of structural materials for fission and fusion reactors. The activation cross section data on (n,2n) reaction for these

isotopes are of practical interest especially for calculating neutron multiplication and neutron transport calculations, in fission and fusion environment.

Thus the present work concentrates on the excitation function of $^{35}Cl(n,2n)^{34m}Cl$, $^{100}Mo(n,2n)^{99}Mo$, and $^{140}Ce(n,2n)^{139}Ce$ reactions to obtain the high quality experimental and theoretical data in terms of accuracy, reproducibility and reliability. The activation technique has been applied in combination with high resolution gamma-ray spectrometry. The statistical model EXIFON and SINCROSS-II have been used in the theoretical evaluation of $^{100}Mo(n,2n)^{99}Mo$, and $^{140}Ce(n,2n)^{139}Ce$ reactions in order to compare experimental measurements with the theoretical predictions.

The present work aims at reducing the existing discrepancies and to provide more accurate activation cross section data of $^{35}Cl(n,2n)^{34m}Cl$, $^{100}Mo(n,2n)^{99}Mo$, and $^{140}Ce(n,2n)^{139}Ce$ reactions in the energy range 13.90 - 14.71 MeV and presenting newer points in between for the first time.

5.2. Experimental Procedure

For the measurement of excitation functions of (n,2n) processes on some isotopes of Cl, Mo, and Ce in the energy range 13.90 - 14.71 MeV, the following salient characteristics are involved:

5.2.1. Sample Preparation and Irradiations

For the determination of (n,2n) cross section of chlorine, molybdenum and cerium isotopes, NaCl (≥99% pure, Fluka Chemica), Mo_2O_3 (≥99% pure, Mark Germany) and CeO_2 (≥99% pure, Mark Germany) in powder form were used as the target for irradiations. The compound NaCl, Mo_2O_3, and CeO_2 contain 60.66%, 79.99%, and 81.41% by weight of chlorine, molybdenum and cerium respectively, and the only other element present is oxygen which gives no interfering background activity. A total of 14 samples were prepared using these compound (5 using NaCl, 4 using Mo_2O_3, 5 using CeO_2). Each sample was pressed at 10 tones/cm^2 into pellets of 1.0 cm diameter and 2 mm thickness. They were sealed in polyethylene cover individually to ensure the mechanical stability. During irradiation each of the sample was sandwiched between two aluminium monitor foils (0.5 mm thick) of the same size as the sample which served as neutron flux monitors. Three individual irradiation were performed for the measurement of (n,2n) cross sections of chlorine, molybdenum and cerium isotopes.

5.2.1.1. Irradiation of NaCl samples

For excitation function measurements of $^{35}Cl(n,2n)^{34m}Cl$ reaction five samples, each sandwiched between pair of aluminium monitor foils, were suspended at 0°, 40°, 70°, 90°,

and 110° with respect to the deuteron beam direction in a ring geometry arrangement as shown in figure 4.1. The five angles cover the neutron energies of 14.71 MeV, 14.57 MeV, 14.31 MeV, 14.10 MeV, and 13.90 MeV which were determined by measuring the ratio of the ^{89}Zr and $^{92m}_{/}Nb$ specific activities produced in Zr and Nb foils by (n,2n) reaction by the D+T neutrons at different angular position[11]. The distance between the sample and neutron target was 6.6 cm. The operational features of neutron generator and irradiation information were as follows:

Deuteron energy	: 110 keV.
Reaction	: $T(d,n)^4He$.
Beam current	: 250 μA.
Beam diameter	: 1 cm
Irradiation time	: 1 hour.

5.2.1.2. Irradiation of Mo_2O_3 Samples

For the measurement of activation cross section of $^{100}Mo(n,2n)^{99}Mo$ reaction, the irradiation with monoenergetic neutrons was done using a D-T neutron generator. In all four Mo_2O_3 samples were used. These were placed at angles 20°, 50°, 70°, and 110° relative to the deuteron beam cover the neutron energies of 14.69 MeV, 14.51 MeV, 14.31 MeV, and 13.90 MeV. The irradiation information are given below:

Deuteron energy	: 110 keV.
Reaction	: $T(d,n)^4He$.
Beam current	: 300 μA.
Beam diameter	: 1 cm
Irradiation time	: 3 hours 40 mins.

5.2.1.3. Irradiation of CeO_2 Samples

A total of five CeO_2 samples, sandwiched with monitor foils, were used to measure the activation cross section of $^{140}Ce(n,2n)^{139}Ce$ reaction. The angles of the irradiation position to the d^+ beam were 0°, 40°, 70°, 90°, and 110° so that the neutron energies of 14.71 MeV, 14.57 MeV, 14.31 MeV, 14.10 MeV, and 13.90 MeV. Following are the operational parameters and irradiation information of neutron generator.

Deuteron energy	: 110 keV.
Reaction	: $T(d,n)^4He$.
Beam current	: 250 μA.
Beam diameter	: 1 cm
Irradiation time	: 3 hours 52 mins.

5.2.2. Neutron Flux Monitor

The neutron flux densities effective at each sample in the irradiation with D-T neutrons were determined only via the monitor reaction $^{27}Al(n,\alpha)^{24}Na$. Use was made of the well known cross section for the reaction $^{27}Al(n,\alpha)^{24}Na$ as standard, with a decay data, as given from Vonach[52] and shown in table 5.1. The small change in flux during the irradiations were, however, recorded by a BF_3 long counter. The average flux values were normalized to the mid count rate at the long counter. The neutron flux densities as given in table 5.2 varied from 0.47787×10^6 to 0.73009×10^6, 0.44064×10^6 to 0.52271×10^6, and 0.42120×10^6 to 0.54436×10^6 for $^{35}Cl(n,2n)^{34m}Cl$, $^{100}Mo(n,2n)^{99}Mo$, and $^{140}Ce(n,2n)^{139}Ce$ reactions respectively.

5.2.3. Activity Measurements

After irradiation, the induced radioactivity of the monitor foils, and the reaction products, was determined by HPGe detector gamma-ray spectrometry. The coaxial HPGe detector has a volume of 98 cm^3 with a resolution 2.66 keV for 1332.51 keV of ^{60}Co gamma-ray source. The spectra were collected for counting times that varied between 15 minutes to several hours. The gamma-ray spectra were acquired by a PC based MCA, S-100 master board packages. The samples were counted on the surface of the detector. The reaction product were identified by their characteristics gamma-ray transition energies and half-lives.

The activity at the end of counting time was found using net area option of the MCA, with automatic subtraction of the background. The activity was subjected to corrections for detection efficiency, dead time, summation effects due to cascade gamma-rays, pile-up losses, and gamma-ray self absorption in the sample. The monitor foils were measured following the measurement for the sample.

5.2..4. Cross Section Calculation and Error Estimation

After determining the disintegration rates of the reaction products at the end of irradiation and their corresponding flux values from the monitor reactions, the cross section values for $^{35}Cl(n,2n)^{34m}Cl$, $^{100}Mo(n,2n)^{99}Mo$, and $^{140}Ce(n,2n)^{139}Ce$ reactions at different energies were calculated using the well known activation formula.

The major sources of errors and their magnitudes are given in table 5.4. The total error of each cross section value was obtained by taking the square root of the sum of squares of the individual errors. The overall uncertainties for all reactions studied in the

present work were in the range of 5-10%. The largest errors in cross sections of reactions determined via gamma-ray spectrometry originated from the poor counting statistics.

5.2.5. Nuclear Model Calculation

In order to describe the measured excitation functions of $^{100}Mo(n,2n)^{99}Mo$ and $^{140}Ce(n,2n)^{139}Ce$ reaction, nuclear model calculations were performed using the computer codes EXIFON and SINCROSS-II. The details of these codes are given in chapter 6.

5.3. Results and Discussion

The results for the (n,2n) cross sections of the investigated nuclides in the energy range from 13.90-14.71 MeV are listed in table 5.3, together with the average neutron energies and its uncertainties, and the spread of the energy distributions. Figures 5.1 through 5.3 display the results of the present work together with those taken from the literature. The cross sections measured in this work are found to be in reasonably good agreement with most recent literature values and to disagree with a few.

Figure 5.1 represents the excitation function of $^{35}Cl(n,2n)^{34m}Cl$ reaction.

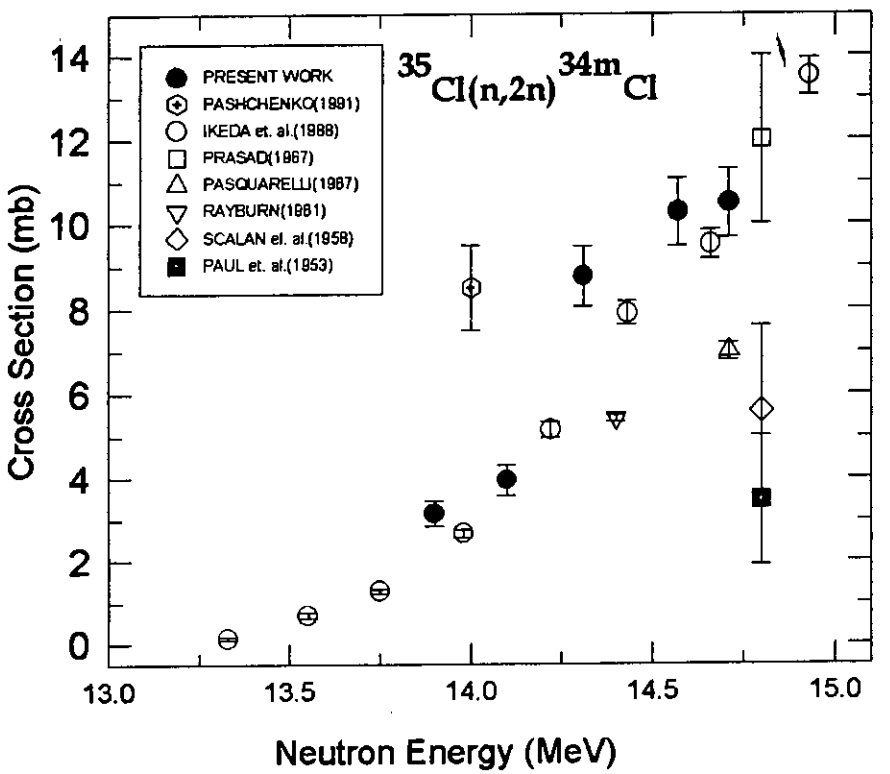

Fig. 5.1. Excitation Function of $^{35}Cl(n,2n)^{34m}Cl$ Reaction.

For this reaction the results of the present work definitely confirm the measurements of Ikeda et. al.[27] and suggested that this work should be used for the whole excitation function rather than the measurements of Paul et. al.[24] and Scalan et. al.[8].

In figure 5.2 is shown the excitation function of $^{100}Mo(n,2n)^{99}Mo$ reaction.

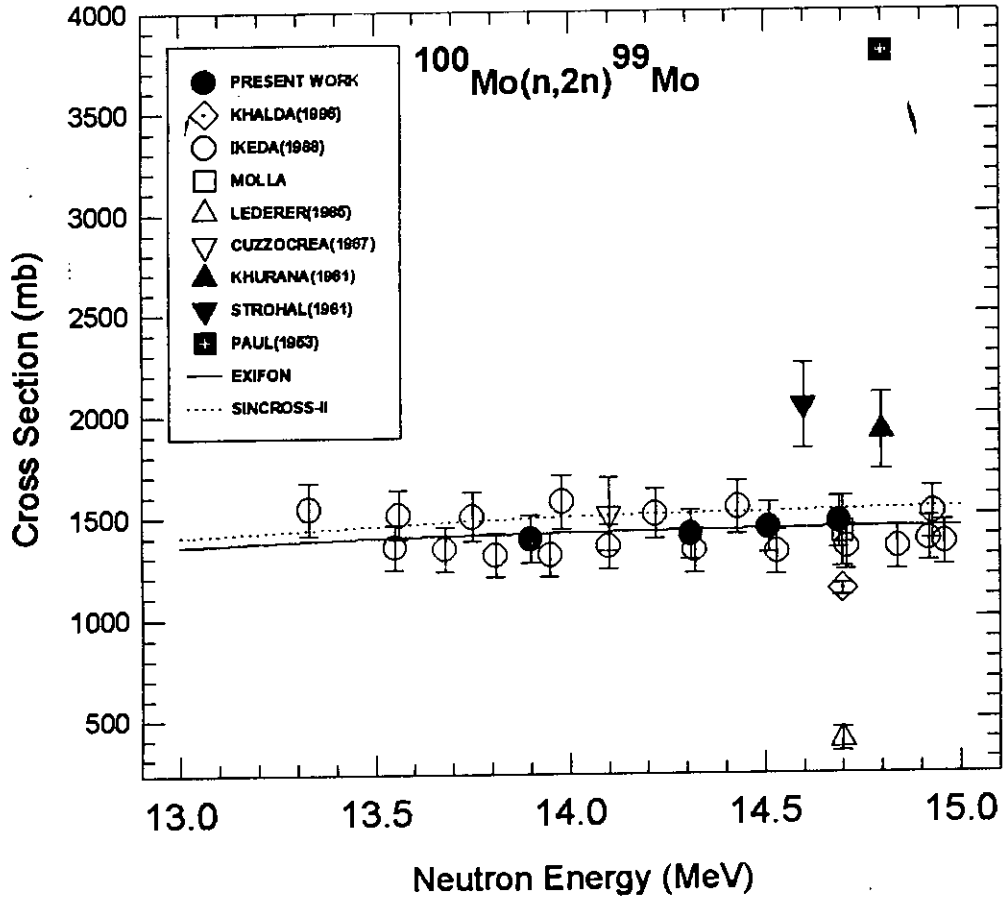

Fig. 5.2. Excitation Function of $^{100}Mo(n,2n)^{99}Mo$ Reaction.

For this reaction the result of the present work agree well with Ikeda et. al.[27]. Most of the other works are inconsistent with each other. These inconsistencies may be attributed to the low isotopic abundance of ^{100}Mo. In this figure a comparison is given between the experimental (n,2n) cross sections measured in this work and the theoretical values obtained using the computer code EXIFON[35] and SINCROSS-II[36]. In general, the results obtained via two computer codes agree and add confidence to the present measurements.

Excitation functions of $^{140}Ce(n,2n)^{139}Ce$ reaction are shown in figure 5.3 with literature and theoretical values.

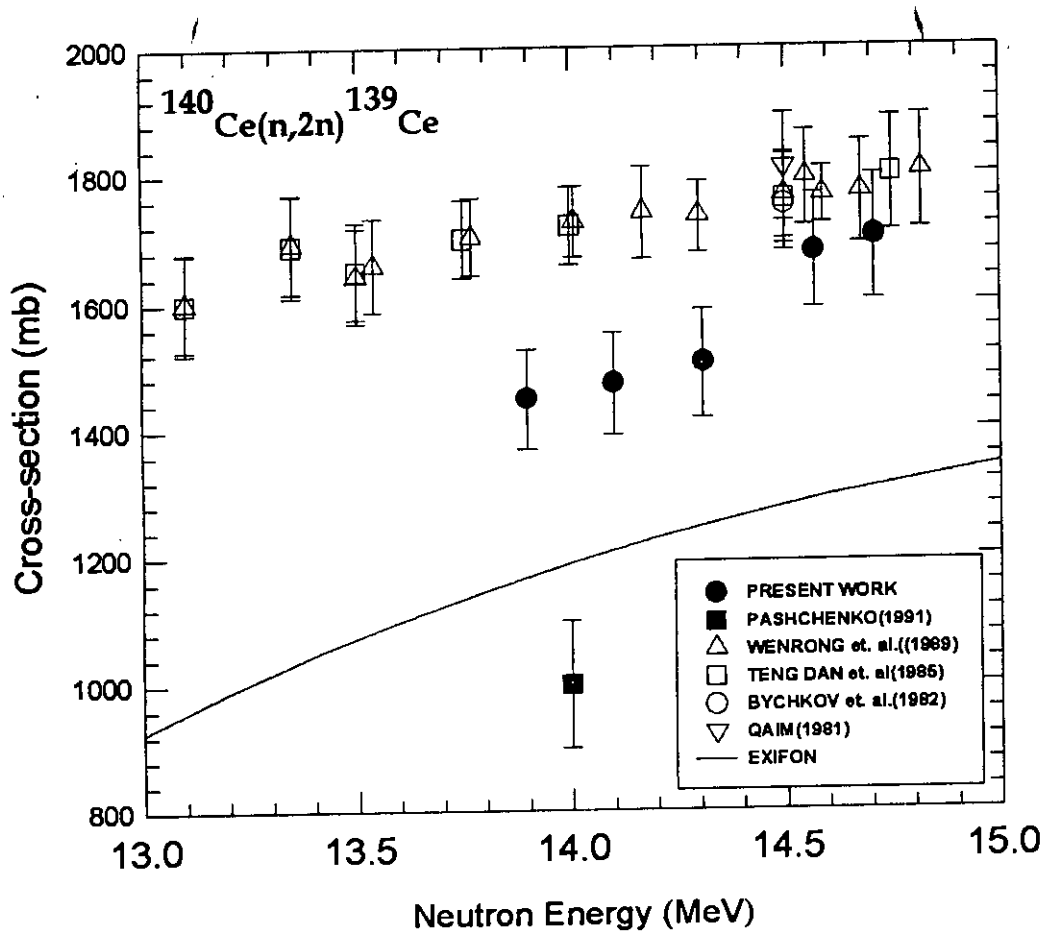

Fig. 5.3. Excitation Function of $^{140}Ce(n,2n)^{139}Ce$ Reaction.

For this reaction the cross sections obtained in the present work are somewhat lower than the results from Wenrong et. al.[17], Teng Dan et. al.[33], Qaim[19], and Bychkov et. al.[20]. In the present work the theoretical values for this reaction using EXIFON are lower than the present experimental value. The literature values from Pashchenko[28] are even less than the present theoretical values. The disagreement was observed in the case of

$^{140}Ce(n,2n)^{139}Ce$ reaction. The difficulty with the measurement of $^{140}Ce(n,2n)^{139}Ce$ reaction cross section may be attributed to the long half-life of the product nucleus of 137.5 days.

The excitation function displays an increase in cross section values with increasing excitation energies above the threshold and reaches a maximum. With further increase in excitation energy more competing reaction channels open resulting in decrease of (n,2n) cross sections.

Table 5.1. Decay data of nuclear reaction products studied in this work [52].

Reaction	Q-value (MeV)	Isotopic abundance (%)	Half-life	γ-energy (keV)	γ-intensity (%)
$^{35}Cl(n,2n)^{34m}Cl$	- 12.646	75.70	32.00 min	145.00	35.80
$^{100}Mo(n,2n)^{99}Mo$	- 8.300	9.60	66.00 h	739.00	14.00
$^{140}Ce(n,2n)^{139}Ce$	- 9.060	88.48	137.50 d	165.90	81.00
$^{27}Al(n,\alpha)^{24}Na$		100.00	15.02 h	1369.00	100.00
				2710.00	100.00

Table 5.2. Reference cross section for monitor reaction $^{27}Al(n,\alpha)^{24}Na$ with measured neutron flux.

Emission Angle (Degree)	Neutron Energy (MeV)	Reference σ (mb)	Neutron Flux ($n.cm^{-2}.sec^{-1}$) $\times 10^6$		
			$^{35}Cl(n,2n)^{34m}Cl$	$^{100}Mo(n,2n)^{99}Mo$	$^{140}Ce(n,2n)^{139}Ce$
0	14.71±0.115	113.1	0.50783		0.54436
20	14.69±0.111			0.51669	
40	14.57±0.108	114.5	0.48175		0.52373
50	14.51±0.095			0.52271	
70	14.31±0.075	119.9	0.47787	0.49231	0.46181
90	14.10±0.041	121.9	0.68423		0.45032
110	13.90±0.045	123.0	0.73009	0.44064	0.42120

Table 5.3. Measured cross sections of (n,2n) reaction on Cl, Mo, and Ce isotopes.

Neutron Energy (MeV)	Cross Section (mb)		
	$^{35}Cl(n,2n)^{34m}Cl$	$^{100}Mo(n,2n)^{99}Mo$	$^{140}Ce(n,2n)^{139}Ce$
14.71±0.115	10.49±0.82		1701±98
14.69±0.111		1466±125	
14.57±0.108	10.28±0.80		1679±89
14.51±0.095		1441±124	
14.31±0.075	8.77±0.71	1407±122	1503±82
14.10±0.041	3.95±0.37		1472±78
13.90±0.045	3.15±0.30	1388±119	1448±70

Table 5.4. Principal sources of errors in neutron induced reaction cross section measurements.

Source of Uncertainty	Magnitude (%)	
	(n,α)	(n,2n)
Neutron Energy	≤ 1	≤ 1
Irradiation time	0.1	0.1
Irradiation geometry and beam deviation	3	3
Sample weight	< 1	< 1
Statistics of counting	10 - 15	3 - 8
Error in peak area analysis	4	3
Efficiency of the detector	5	5
Decay data	1	2
Error in monitor reactions	3 - 8	3 - 8
Neutron absorption and scattering with in the sample	0.5	0.5
Self absorption of gamma-ray in sample	0.5	0.5
Total error	13 - 19	8 - 13

CHAPTER-6

THEORETICAL CALCULATION CODES FOR ACTIVATION CROSS SECTION EVALUATION IN THE NEUTRON ENERGY REGION 13 - 15 MeV

Theoretical Calculation Codes for Activation Cross Section Evaluation in the Neutron Energy Region 13 - 15 MeV

6.1. Introduction

Theoretical calculation of activation cross sections plays an important role in nuclear data evaluations. Evaluation of activation cross section in the neutron energy region 13-15 MeV are necessary in a lot of applications such as accelerator shielding calculation, production rate estimation of medical radioactive isotopes and radiation damage in fission and fusion devices. A large number of activation cross section measurements have been performed, and various efforts have been devoted to make comprehensive nuclear data evaluations such as JENDLE-3[22], ENDF/B-V[45], -VI[21], IRDF-90[53]. There are however large discrepancies for certain reactions among the experimental data measured by various groups using different techniques, neutron sources and decay data. In some cases the data are scarce. Although nuclear data evaluators have attempted to provide the reasonable evaluations, it is impractical to provide reliable cross section values when the data scatter widely or when there are few measured values. Therefore, there are still strong needs for measured activation cross section data with uncertainties less than 10%.

Several theoretical codes are considered to be candidate for activation cross section data evaluation in the neutron energy region 13-15 MeV. However, before performing an intensive evaluation, it is worthwhile to make cross section calculations in order to check the advantages and limitations of those codes which are based on different theories, approximations and methods of numerical calculations.

There are several theoretical codes available to calculate Nuclear Data. Selected codes were SINCROSS-II[36], ALICE-F[54], EXIFON[35], MCEXCITON [55], NUCLEUS[56], and HETC-3 STEP[57-59]. The first three of these codes employ deterministic methods, while

the last three codes are based on the Monte-Carlo method. In the present experiment two codes SINCROSS-II and EXIFON were used to calculate the activation cross section values in the neutron energy range 13-15 MeV. In this chapter some explanations are made for theories, models, assumptions and parameters on which SINCROSS-II and EXIFON codes are based.

6.1.1. SINCROSS-II - A - Nuclear Cross Section Calculation System With Simplified Input-Format

6.1.1.1. Introduction

The SINCROSS-II is a revised version of the SINCROSS-I[60]. The main codes of SINCROSS-II are the ELIESE[61] - GNASH[62] joint program (EGNASH2) and the simplified input version of DWUCKY[63]. To aim the efficient execution of nuclear cross section calculations, both the codes, ELIESE and GNASH were joined and the global optical potentials were built into the new code EGNASH, whose input-format become simpler than that of GNASH.

EGNASH2 calculates the nuclear cross sections over the wide mass region using the built-in optical-model potential parameters. The code EGNASH2 has a few free parameters for the pre-equilibrium process, level density, and radiative width.

Since many of the parameters were predetermined and stored in the program, the parameters which should be inputted are a small number. A sample unit is given in table 6.2.

6.1.1.2. Optical-Model Potential Parameters

In the statistical nuclear model, the angular momentum dependent particle transmission coefficients are calculated by optical-model potential parameters. In the SINCROSS, as a general rule, the global optical-model potentials are employed to calculate the transmission coefficients.

For the neutron, a modified Walter-Guss-Potential[64] and the Wilmore-Hodgson[65] potential parameters are built into the EGNASH2. Walter-Guss recommend their potential to be applied above 53 in mass-number and 10 to 80 MeV in energy range. To apply the potential below 10 MeV neutron energy, the following surface absorption term Ws (in MeV) is assumed between 0 to 20 MeV,

$$W_s = 7.71 - 14.94(N - Z)/A \quad \text{----------(6.1.1)}$$

6.1.1.3. Level Density and Gamma-ray Transition Parameters

In the continuum level region, the Fermi-gas and the constant temperature model are used to represent the level density of nucleus. The Fermi-gas model formula as a function of energy E and spin J is

$$\rho\ (E,J) = \frac{\exp\{2[a(E-\Delta)]^{\frac{1}{2}}\}}{C_0(E-\Delta)^2} R(J,E) \quad \text{----------(6.1.2)}$$

where $C_o = 24\sqrt{2}(0.146)^{\frac{3}{2}} a\ A$, and the spin term is given by

$$R(J,E) = (2J+1)\exp[\frac{-(J+\frac{1}{2})^2}{\{2\sigma^2(E)\}}] \quad \text{----------(6.1.3)}$$

where σ^2 (E) is the spin cutoff factor defined by

$$\sigma^2(E) = 0.146\ [a\ (E-\Delta)]^{\frac{1}{2}} A^{\frac{2}{3}} \quad \text{----------(6.1.4)}$$

The pairing correction Δ was quoted from the Gilbert and Cameron's paper[66].

In the lower excitation, the constant temperature formula expressed by

$$\rho\ (E,J) = \rho\ (E_x)\exp[(E - E_x)/T]\ R(J,E),\ \ E\langle E_x \text{ ----------(6.1.5)}$$

is used, where E_x is the energy at which both densities are smoothly connected, and $\rho(E_x)$ is the energy term of level density at the energy E_x. If the spin dependent level density $\rho(E,J)$ is summed over the spin J, we get the density $\rho(E)$ of levels of all J, which has a different form from the constant temperature formula of Gilbert and Cameron[66], as the spin cutoff factor $\sigma^2(E)$ is energy dependent.

The GNASH code[62] is able to automatically determine the nuclear temperature, T, if the discrete levels in the low energy region and the Fermi-gas level density parameters "a" were suitably inputted. Then the level density of nucleus in the continuum can be described by the parameter "a" only. In some cases, however, the code is unable to match discrete levels, and thus the temperature, which connects smoothly between the Fermi-gas and discrete levels, is not determined. For those cases, the temperature is calculated with a systematic relation between level density parameter and temperature,

$$T = 7.50 \times a^{-0.84} \text{ ----------(6.1.6)}$$

At the beginning of the calculation, when the experimental value of the average spacing D_0 of S-wave neutron resonances at the neutron binding energy E_B is known[67], the parameter "a" was assumed to have a value which is calculated from the spacing D_0 by inversely solving the equation[68].

$$D_0 = C_0(E_B - \Delta)/(2I+1)\ \exp\ [(3+(2I+1)^2)/(8\sigma^2(E_B))\ - 2\sqrt{a(E_B - \Delta)}] \text{----6.1.7)}$$

where I is the spin of target nucleus and a set of parameters "a" of isotopes in the nuclear decaying processes has practically been selected through the cross section calculation to agree with the various experimental data which could be considered to be reliable.

The relation between the level density parameter "a" and the total shell correction S given by Gilbert and Cameron[66] and the tentative formula,

$$\frac{a}{A} = 0.008\ S + 0.170 \quad \text{----------(6.1.8)}$$

is programmed to give the initial value of "a" for the undeformed nuclei for which the cross section is not yet calculated.

In the mass region A<20, in which Gilbert and Cameron did not give Δ and S, it is assumed that $\Delta = \frac{11}{\sqrt{A}}$ for odd-mass nuclei, and $\Delta = \frac{22}{\sqrt{A}}$ for even-even nuclei, and the shell correction energy $S = M_{exp} - M_{1\,dp}$, where M_{exp} and $M_{1\,dp}$, are the experimental nuclear mass and the calculated nuclear mass using the mass formula of the liquid-drop model, respectively.

6.1.1.4. Determination Procedure for the Value of Parameters

In the SINCROSS, the global optical-model potential parameters are employed to calculate the transmission coefficients, as mentioned in section 6.1.1.2 The key points of the cross section calculation, therefore, are the determination of level density parameters of daughter nuclei and of the rate of contribution of pre-equilibrium and direct processes to the statistical process. In the following, the method of parameter determination of the pre-equilibrium process and for the level density is described in detail at subsections 6.1.1.5 and 6.1.1.6 respectively.

6.1.1.5. Parameter Determination of the Pre-equilibrium Process

In the code EGNASH2, the pre-equilibrium and direct processes of particle emission are treated with the code PRECO developed by Kalbach[69], which is coupled with GNASH, and with the code DWUCKY for the inelastic-scattering. In the GNASH, the single particle state density and the normalization factor for exciton model were free parameters. In contrast with this, the single-particle state density constant is not free, but related to the level density parameter "a" by the formula,

$$g = (\frac{6}{\pi^2})a \quad \text{----------(6.1.9)}$$

In the EGNASH2, in addition to the normalization factor F2, which is equal to the Kalbach constant divided by 100, adjusting factors F3 and F4 are introduced for pick-up and knock-out processes, respectively.

6.1.1.6. Parameter Determination of the Level Density

After the parameters for the pre-equilibrium and direct processes were selected, the free parameter to be determined is only the level density parameter "a" in the Fermi-gas model, because the nuclear temperature used in the constant temperature model can be determined automatically or by the equation (6.1.6). Since the total emission of various kinds of particles from the compound nucleus is controlled by a set of level density parameters for daughter nuclei, it is better that the level density parameter of each daughter nucleus is so practically determined that the calculated cross sections for reactions, (n,2n), (n,p), and (n,α) agree with the experimental data of respective reactions.

The first step to fix the level density parameters is to calculate these using the experimental value of mean level spacing for S-wave neutron resonances at the neutron binding energy. The calculation was made by solving inversely equation (6.1.7), with the spin cutoff-factor defined by equation (6.1.4) and the pairing correction quoted from Gilbert and Cameron[66].

The second step to determine the level density parameters is the cross section calculation in the mass region where the reliable experimental data exist. The level density parameters with half-life and spin for $^{63}Cu(n,\alpha)^{60}Co$ and $^{100}Mo(n,2n)^{99}Mo$ reactions are given in table 6.1.

6.1.1.7. Calculation of Activation Cross Section using EGNASH2 and Comparison between Calculated and Experimental Values

The code EGNASH2 has a few parameters for the equilibrium process, level density, and radiative width. Several test calculations of cross sections in the energy range 13-15 MeV were carried out referring to the experimental data for the (n,2n) and (n,α) reactions of molybdenum and copper. The cross section of $^{100}Mo(n,2n)^{99}Mo$ reaction depends on the level density parameter and radiative width of ^{100}Mo isotope as the target nucleus of the reaction, and that of $^{63}Cu(n,\alpha)^{60}Co$ reaction depends on level density parameters of Cu isotope as the target nucleus.

The measurement of cross sections of molybdenum and copper isotopes, performed by Ikeda et al.[27] and Konno et al. [16] , are very useful for the determination of level density parameters. The cross section calculations for the isotopes ^{60}Co and ^{100}Mo, were performed using the level density parameters. The results of calculations were compared with the experimental data and shown in figures 4.3 and 5.2. To fit well with the experimental cross

sections for the reactions $^{63}Cu(n,\alpha)^{60}Co$ and $^{100}Mo(n,2n)^{99}Mo$, the radiative widths of ^{60}Co and ^{100}Mo isotopes were adjusted.

Table 6.1. Level density parameters with half-life and spin

Reactions	Level Density Parameters "a".	Half-life	Spin "J"
$^{63}Cu(n,\alpha)^{60}Co$	9.5	5.27 y	5^+
$^{100}Mo(n,2n)^{99}Mo$	17.9	66.00 h	$1/2^+$

Table 6.2. Sample of input data $^{63}Cu(n,\alpha)^{60}Co$ reaction.

```
Cu63n2
Cu-63   +   NEUTRON  REACTION   (ELIESE-GNASH JOINT PROGRAM EGNASH2)
                                                  1997 02 14  S.M. HOSSAIN
  6      0    11          0       0      1     8      -1       1
1.          29063.              0.5              0.8                              0.1
0.0586
   5
13.0          13.5          14.0          14.5          15.0
29065.        5.
29063.        3.
29062         1.
28063         2.
28062         1.
27060         1.
0.
0.
0.
27060         2
```

6.1.2. EXIFON - A Statistical Multistep Direct and Multistep Compound Reaction Model

6.1.2.1. Introduction

H. Kalka has written the EXIFON[35] code based on an analytical model for the description of excitation function of (n,α), (n,2n) and (n,p) reactions within a statistical multistep direct and multistep compound reactions (SMD/SMC) model. The theoretical calculations for $^{100}Mo(n,2n)^{99}Mo$ and $^{140}Ce(n,2n)^{139}Ce$ reactions have been performed in the neutron energy range 13-15 MeV following statistical multistep direct and statistical multistep compound reaction model.

For the comparison of experimental values with the theoretical one, EXIFON code was used in the energy range 13-15 MeV in step of 0.20 MeV.

The code predicts emission spectra, angular distributions and activation cross-sections including equilibrium, pre-equilibrium, as well as direct (collective and non-collective) processes. Multiple particle emissions are considered up to three decay modes of the compound system. The model is restricted to neutron, proton and α-induced reactions with neutrons, protons, alphas, photons in the outgoing channels. The range of validity : target mass numbers A>20, bombarding energies below 100 MeV. The cross-sections for the reactions $^{100}Mo(n,2n)^{99}Mo$ and $^{140}Ce(n,2n)^{139}Ce$ calculated by the code EXIFON along with the experimental cross-section values have been plotted in figures 5.2 and 5.3.

6.1.2.2. The Statistical Multistep Reaction Models

A unique description of (a,xb) emission spectra where a,b = n,p,α and γ (neutron, proton, alpha, and γ-ray) as well as excitation functions (activation cross-sections) is proposed within a pure statistical multistep reaction model[70-73]. This approach is based on many body theory (green's function formalism)[74-77] and random matrix physics[78,79]. In the statistical multistep reaction model the total emission spectrum of the process (a,xb) is divided in three main parts: (a,xb) = (SMD)+ (SMC) + (MPE)

or

$$\frac{d\sigma_{a,Xb}(E_a)}{dE_b} = \frac{d\sigma_{a,b}^{SMD}(E_a)}{dE_b} + \frac{d\sigma_{a,b}^{SMC}(E_a)}{dE_b} + \frac{d\sigma_{a,Xb}^{MPE}(E_a)}{dE_b} \quad \text{.....(6.2.1)}$$

The first term on the right hand side denotes the statistical multistep direct (SMD) part which contains from single-step up to five-step contributions. Besides particle-hole excitations collective phonon excitations are also considered. The second part symbolizes the statistical multistep compound (SMC) emission which bares on a master equation. Both terms taken together (SMD+SMC) represent the so called first-chance emission process. In the last term, multistep particle emission (MPE) reactions which include the second-chance, third-chance emissions, etc. are summarized, i.e,

$$\frac{d\sigma_{a,xb}^{MPE}(E_a)}{dE_b} = \Sigma_c \frac{d\sigma_{a,cb}(E_a)}{dE_b} + \Sigma_{c,d} \frac{d\sigma_{a,cdb}(E_a)}{dE_b} + \text{.....(6.2.2)}$$

6.1.2.3. Activation Cross-sections

The following (model-independent) reactions between the optical model (OM) reaction cross-section and the energy-integrated particle cross-sections should be satisfied (at each incident energy E_a)

$$\sigma_a^{om} = \sum_b \sigma_{a,b} \quad \text{.....(6.2.3)}$$

$$\sigma_{a,b} = \sum_c \sigma_{a,bc} \text{ and } \sigma_{a,bc} = \sum_d \sigma_{a,bcd} \quad \text{.....(6.2.4)}$$

with $\sigma_{a,b} = \sigma_{a,b}^{SMD} + \sigma_{a,b}^{SMC}$, the total first-chance emission. In this context, activation cross-sections are given by

$$\sigma_{a,b\gamma} = \sigma_{a,b} - \sum_{c\neq\gamma} \sigma_{a,bc} \quad \text{.....(6.2.5)}$$

$$\sigma_{a,cb\gamma} = \sigma_{a,cb} - \sum_{d\neq\gamma} \sigma_{a,cbd} \quad \text{.....(6.2.6)}$$

where $b,c,d \neq \gamma$. For example, (n,α), (n,2n), and (n,p) activation cross sections can be expressed in the following form:

$$\sigma_{n,\alpha\gamma} = \sigma_{n,\alpha} - \sigma_{n,\alpha n} - \sigma_{n,\alpha p} - \sigma_{n,2\alpha} \quad \text{.....(6.2.7)}$$

$$\sigma_{n,2n\gamma} = \sigma_{n,2n} - \sigma_{n,3n} - \sigma_{n,2np} - \sigma_{n,2n\alpha} \quad \text{.....(6.2.8)}$$

$$\sigma_{n,p\gamma} = \sigma_{n,p} - \sigma_{n,pn} - \sigma_{n,p\alpha} \quad \text{.....(6.2.9)}$$

6.1.2.4. Model Parameters of EXIFON

The following abbreviation have been used in the model parameters of EXIFON code :

Excitation energies of the composite system,

$$E = E_a + B_a$$

Excitation energies of the residual system ,

$$U = E_a + B_a - B_b - E_b$$

Binding energies of the ingoing (c=a) particle = B_c

Kinetic energies of the outgoing (c= b) particle,

$$E_c = \frac{\hbar K_c}{2\mu}$$

To keep the model tractable a simple two-body interaction first proposed by Green and Moszkowski[80] and then A. Faessler[81],

$$I(r_1,r_2) = -4\pi \frac{F_0}{A} [\chi nl(R)]^{-4} \delta(r_1-r_2)\delta(r_1-R) \quad \text{.....(6.2.10)}$$

with F_0 = 27.5 MeV taken from nuclear structure considerations. This surface delta force is separable and can be interpreted[77] as an idealized density dependent force. Due to the factor $[\chi nl(R)]^{-4}$, which contains the wave functions at the nuclear radius $R = r_0 A^{1/3}$, the matrix elements becomes state dependent. Thus the simple analytical expressions for the mean squared matrix elements between bound configurations[73] is

$$\bar{I}^2_{BB} = 2^{-5} (F_0/A)^2 (k_F R)^{-2} \quad \text{.....(6.2.11)}$$

with $\hbar k_F$ and E_F are the Fermi momentum and Fermi energy respectively. All other types of mean squared matrix elements between bound and /or unbound configurations are simply related to I_{BB},

$$\bar{I}^2_{BU}(E_b) = [\delta_{bn} + \delta_{bp} + 2F_{13}(E_b)\,\delta_{b\,\alpha}(2S_b+1)\,\frac{\rho(E_b)}{2}\;\bar{I}^2_{BB}. \quad \text{.....(6.2.12)}$$

$$\bar{I}^2_{UB}(E_a) = (4\pi)^{-1}\,\frac{\rho(Ea)}{2}\,\frac{E_F}{E}\;\bar{I}^2_{BB} \quad \text{.....(6.2.13)}$$

$$\bar{I}^2_{UU}(E_a,E_b) = (4\pi)^{-1}\,\frac{(2S_b+1)}{(2S_a+1)}\,\frac{\rho(Ea)}{2}\,\frac{\rho(E_b)}{2}\,\frac{E_F}{E_a}\,4\;\bar{I}^2_{BB} \quad \text{.....(6.2.14)}$$

The single particle state density of particles c= n,p,α with mass μ_c is given by

$$\rho(E_c) = 4\pi\, v\, \mu_c\, (2\mu_c\, E_c)^{1/2}/\,(2\pi\hbar)$$
$$= (4.48\text{x}10^{-3}\ \text{fm}^{-3}\ \text{MeV}^{-3/2})\, r_0^3\, A\, E_c^{\,1/2} \quad \text{.....(6.2.15)}$$

where $V= 4\pi R^3/3$ is the nuclear volume. The single particle state density of bound particles (at Fermi energy) is then defined by

$$g= 4\rho\,(E_F) \quad \text{.....(6.2.16)}$$

where the factor 4 considered the spin and isospin degeneracy. In equation (6.2.12) the dependence on particle type b is explicitly shown. For α-particles the (1,3) formation mode is given by

$$F_{13}\,(E_\alpha)= 0.28144-0.01113E_\alpha + 1.34\text{x}10^{-4}E\alpha^2 \quad \text{.....(6.2.17)}$$

where, E_α in MeV was taken from pairing effect.

Pairing effects are considered by using effective binding energies B_c^{eff}. For a system of A = N+Z nucleons the effective neutron (proton) binding energy is defined by

$$B_n^{eff} = B_n \pm \Delta \quad \text{for} \quad \begin{pmatrix} odd \\ even \end{pmatrix} N \qquad \text{.....(6.2.18)}$$

$$B_p^{eff} = B_p \pm \Delta \quad \text{for} \quad \begin{pmatrix} odd \\ even \end{pmatrix} Z \qquad \text{.....(6.2.19).}$$

where $B_{n(p)}$ is the experimental neutron (proton) binding energy. The pairing shift is $\Delta = 12.8\ A^{-1/2}$ MeV taken from[82]. For α-and γ-emissions $B_\alpha^{eff} = B_\alpha$ and $B_\gamma^{eff} = 0$ were considered. It may be noted that by definitions (6.2.18) and (6.2.19), all odd-even effects cancel. In SMD processes effective binding energies are used in the outgoing channels only (pairing effects are not considered for phonon excitations). In MPE we have, for example, for the (a,cb) process,

$$B_c^{eff} + B_b^{eff} = B_c + B_b + D^{eff} \qquad \text{.....(6.2.20)}$$

where the effective pairing shift D^{eff} according to equations (18) and (19) can be -2Δ, $-\Delta$, 0, Δ or 2Δ depending on the reaction channel (a,cb).

6.1.2.5. Statistical Multistep Direct (SMD) Cross Sections

The SMD cross-section can be expressed as a sum over S-step direct process,

$$\frac{d\sigma_{a,b}^{SMD}(E_a)}{dE_b} = \sum_{S=1} \frac{d\sigma_{a,b}^{(S)}(E_a)}{dE_b} \qquad \text{.....(6.2.21).}$$

for example, the single and two step processes are defined by

$$\frac{d\sigma^{(1)}_{a,b}(E_a)}{dE_b} = \frac{(2\pi)^4}{K_a^2} W_{ab}(E_a, E_b) \quad \text{.....(6.2.22).}$$

$$\frac{d\sigma^{(2)}_{a,b}(E_a)}{dE_b} = \frac{(2\pi)^4}{K_a^{(2)}} \sum_C \int_{E_b}^{E_a} dE_1 W_{ac}(E_a, E_1) 2\pi^2 W_{cb}(E_1, E_b) \quad \text{.....(6.2.23)}$$

Besides particle-hole excitations[ex] the transition probability in equations (6.2.22) and (6.2.23) also includes collective excitations[vib],

$$W_{ab} = W_{ab}^{[ex]} + W_{ab}^{[vib]} \quad \text{..... (6.2.24)}$$

Thus, the SMD cross section is a sum of the following contributions denoted according to the sequence of exciton and phonon excitations: [ex], [vib], [2ex], [ex, vib], [vib,ex], [2vib], [3ex], [4ex], and [5ex]. For S≥3, phonon excitations are neglected, since they are proved to be negligible. For α-particles in the outgoing channel the SMD cross section is multiplied by equation (6.2.17).

6.1.2.6. Statistical Multistep Compound (SMC) Cross Section

The SMC cross section has the familiar form (b=n,p,α,γ)

$$\frac{d\sigma^{SMC}_{a,b}(E_a)}{dE_b} = \sigma_a^{SMC}(E_a) \sum_{N=N_0}^{N'} \frac{\tau_N(E)}{\hbar} \sum_{(\Delta N)} \Gamma^{(\Delta N)}_{N,b}(E, E_b)\uparrow \quad \text{.....(6.2.25)}$$

where $\tau_N(E)$ satisfies the time-integrated master equation

$$-\hbar\delta NN_0 = \Gamma^{(+)}_{N-2}(E)\downarrow \tau_{N-2}(E) + \Gamma^{(-)}_{N+2}(E)\downarrow \tau_{N+2}(E) - \Gamma_N(E)\tau_N(E) \text{.....(6.2.26)}$$

For each exciton number $N=N_p+N_h$, the sum in equation (6.2.25) runs from N_0 up to a reliable maximum N' which includes the so called "equilibrium stage" $\overline{N} \approx (1.4gE)^{\frac{1}{2}}$. The initial exciton number is N_0=2,3, or 6 phonon-, nucleon-, or α-induced reactions. The damping widths are defined by

$$\Gamma^{(\Delta N)}_N(E)\downarrow = 2\pi\ \bar{I}^2_{BB}\rho^{(\Delta N)}_N(E) \text{ .....(6.2.27)}$$

with the corresponding final state densities for the two modes ΔN = 2 and -2,

$$\rho^{(+)}_N(E) = \frac{7}{8}g^3E^2\ /(N+1) \text{ .....(6.2.28)}$$

$$\rho^{(-)}_N(E) = \frac{7}{8}gN_pN_h(N-2) \text{ .....(6.2.29)}$$

The partial escape widths are given by

$$\Gamma^{(\Delta N)}_{N,c}(E,E_c)\uparrow = 2\pi\ \bar{I}^2_{BU}(E_c)\rho^{(\Delta N)}_{N,c}(E,U) \text{ .....(6.2.30)}$$

With the modes for the (particle) emission (c=n,p,α)

$$\rho^{(+)}_{N,c}(EU) = \frac{7}{8}(\frac{N_h}{N})g^2E(\frac{U}{E})^{N-2}[(N-1)-(N-2)(\frac{U}{E})] \text{ .....(6.2.31)}$$

$$\rho^{(-)}_{N,c}(EU) = \frac{7}{16}N_pN_h(N_p-1)\frac{(N-1)!}{(N-4)!}\frac{1}{E}(\frac{U}{E})^{N-4}[1-(\frac{U}{E})] \text{ .....(6.2.32)}$$

Further, the integral and the total widths are defined by

$$\Gamma_N^{(\Delta N)}(E)\uparrow = \sum_c \int dE_c \Gamma_{N,c}^{(\Delta N)}(E, E_c)\uparrow \quad \text{.....(6.2.33)}$$

$$\Gamma_N(E) = \sum_{(\Delta N)} [\Gamma_N^{(\Delta N)}(E)\downarrow + \Gamma_N^{(\Delta N)}(E)\uparrow] \quad \text{.....(6.2.34)}$$

The sum in equation (6.2.33) runs over all particle-types c=n, p, α, and γ.

6.1.2.7. General Features and Standard Parameter Set of EXIFON

General features and parameters used in the EXIFON code for the measurement of activation cross section are summarized below:

General Features

Computer	: 486, IBM PC-AT (Model: AT/486, Speed: 33 MHz)
Language	: FORTRAN 77
Characters	: ASCII (IBM International Graphic)
Memory Size	: 300 K Byte
No. of Subroutines	: 13
Records	: about 1600
Running time	: about 15 sec per incident energy (depends on the computer speed)

Standard Parameter Set

Strength of surface delta interaction[81]	: F_0 = 27.5 MeV
Radius Parameter[83]	: $r_0 = 1.21 + 4.0\ A^{-2/3} - 15\ A^{-4/3}$
Potential Depth[84]	: $V_0 = 52 - 0.3\ E_a$ MeV
Fermi Energy	: E_F = 33 MeV
Pairing Shift[82]	: $\Delta = 12.8\ A^{-1/2}$ MeV
Phonon (Breit-Wigner) Width	: $\Delta\omega$ = 1.4 MeV
Optical Model Potential[85]	: For neutrons - Wilmore-Hodgson
	For alphas - Huizenga-Igo
	For protons - Perey et. al.

Theoretical cross section calculations for $^{100}Mo(n,2n)^{99}Mo$ and $^{140}Ce(n,2n)^{139}Ce$ reactions using EXIFON code, the following parameters were changed to obtained the better cross section values in the neutron energy range 13-15 MeV: strength of residual interaction F_o, radius parameter r_o, Fermi energy E_F, phonon width ω_λ and the global Optical Model parameter set for protons.

CHAPTER-7

CONCLUSIONS

Conclusion

Activation cross section measurements have been carried out in a unified experimental condition at neutron energy range from 13.82-14.71 MeV using D-T neutron source at neutron generator facility in Atomic Energy Research Establishment, Savar in order to provide substantial data base supporting the nuclear design of fusion reactors. Excitation functions of $^{35}Cl(n,2n)^{34m}Cl$, $^{63}Cu(n,\alpha)^{60}Co$, $^{100}Mo(n,2n)^{99}Mo$, and $^{140}Ce(n,2n)^{139}Ce$ reactions have been reported from the present work.

The theoretical calculations of the excitation functions have been done in the neutron energy range 13 - 15 MeV for the reactions $^{63}Cu(n,\alpha)^{60}Co$, $^{100}Mo(n,2n)^{99}Mo$, and $^{140}Ce(n,2n)^{139}Ce$. The calculations have been done using the computer codes SINCROSS-II and EXIFON. In most of the cases the agreement between experiment and theory is satisfactory. In general, the results obtained using two codes agree and add confidence to the present experiments.

The present experimental data showed significant improvement in accuracy in comparison with earlier reported data. As such, the data obtained from the present work will offer considerable nuclear data base for fusion reactor technology design, current evaluation of neutron activation cross section, applied nuclear theory, nuclear model calculations for nuclear technology applications, understanding irradiation damage, waste treatment and maintenance of the facility.

CHAPTER-8

REFERENCES

References

1. O.Hahn and F. Strassmann, Naturewissenschaften, 27 (1939) 11.

2. J. Csikai, Proc. of the advisory group meeting on nuclear data for fusion reactor technology, Vienna, 11-15 Dec. 1978, IAEA-TECDOC 223 (1979) 199.

3. J. Csikai, Handbook of Fast Neutron Generator, vol. 1, CRC press, USA (1987).

4 D.E. Cullen et. al., The International Reactor Dosimetry File (IRDF-82), IAEA-NDS-42/R (1982)

5. V. Seki, H. Iida, H. Kawasaki, Graphical representation of transmutation and decay chain data transmutation cross section and delayed gamma-ray emission data, JAERI-1280 (1982).

6. B.P. Evain, D.L. Smith, P. Lucchese, Compilation and evaluation of cross section for nuclear technology and applications, ANL/NDM-89 (1985).

7. R. Prasad and D.C. Sarkar, NP A94 (1967) 476-480.

8. R.S. Scalan, R.W. Fink, NP 9 (1958) 334-336.

9. Khalda, T. Osman and F.I. Habbani, INDC(SUD)-001/L, IAEA, Vienna, October (1996).

10. M. Lederer and Virginia S. Shirley, Table of Isotopes, Seventh Edition (1985).

11. R.U. Miah, Ph.D. thesis (submitted for Ph.D. degree), Dhaka University.

12. Proc. second ASTM-EURATOM Symp, Reactor Dosimetry, Dosimetry methods for fuels, cladding, and structural materials, Palo Alto, California, October, 3-7 (1977)

13. J. Csikai, Nucl. Instrm. Meth. in Phys. Research A280 (1989) 233.

14. N.B. Perez, E.T. Cheng, A.B. Pashchenko, H.K. Vonach, INDC(NDS)-302, IAEA, Vienna, Austria, April (1994).

15. A. paulsen et. al. Nucleonik, 10 (1961) 91.

16. Chikara Konno, Yujiro Ikeda, Koji Oishi, Kiyoshi Kawade, Hiroshi Yamamoto, and Hiroshi Maekawa, JAERI 1329, October (1993) 32.

17. Zhao Wenrong, Lu Hanlin, Yu Weixiang and Yuan Xialin, INDC(CPR)-16, IAEA, Vienna, August(1989) 40.

18. J. Csikai, C.S.M. Buezko, R. Pepelnik, and H.M. Agrawal, INDC(NDS)-232/L, IAEA, Vienna, January (1990) 61.

19. S.M. Qaim, Handbook of spectroscopy, vol. III, CRC Press Inc. Boca Raton, Florida (1981) 141.

20. V.M. Bychkov, V.N. Manokhin, A.B. Pashchenko and V.I. Plyaskin, Cross sections for neutron induced threshold reactions, Energoizdat, Moscow (1982).

21. ENDF/B-VI Summary Documentation, Compiled by P.F. Rose, ENDF-201, 4th Edition, Brookhaven National Laboratory (1991).

22. Japanese Evaluated Nuclear Data Library, Version-3, JENDLE-3, JAERI 1319, June (1990).

23. M. Bormann et al., EANDC (E)-150 (1972) 30.

24. E.B. Paul and R.L. Clarke, Can. J. Phys. 31 (1953) 267.

25. A. Pasquarelli, NP 9 (1958) 334.

26. L.A. Rayburn, PR vol. 122, No. 1, April (1961) 168.

27. Y. Ikeda, C. Konno, K. Oishi, T. Nakamura, H. Miyade, K. Kawade, H. Yamamoto, and T. Katoh, JAERI 1312, March (1988).

28. A.B. Pashchenko, INDC(CCP)-323/L, IAEA, Vienna, January (1991).

29. N.I. Molla, M.M. Rahman, INDC (BAN)-003/Cr, INT (86)-8.

30. P. Cuzzocrea, E. Perillo, and S. Notarrigo, NP A103 (1967)616-624.

31. C.S. Khurana and H.S. Hans, NP 28 (1961) 560.

32. P. Strohal, N. Cindro, and B. Eman, NP 30 (1961) 560.

33. Teng Dan, et. al., CNP, 4, (1985) 307.

34. R.G. Wille and R.W. Fink, PR 118 (1960) 242.

35. H. Kalka, EXIFON- A statistical multistep reaction code, Technische Universitat Dresden, G.D.R., May (1990). Private communication.

36. N. Yamamuro, A Nuclear Cross Section Calculation System With Simplified Input-Format, Version-II, SINCROSS-II, JAERI-M 90-006, NEANDC(J)-146/U, INDC(JPN)-133/L, February (1990).

37. Saadia Amiel, Nondestructive Activation Analysis, Elsevier Scientific Publishing Company (1981).

38. J.C. Laul, Neutron Activation Analysis of Geological Materials, Atomic Energy Review, USA, 173 (1979).

39. Herman Cember, Introduction to Health Physics, Second Edition, Pergamon Press (1989).

40. Gordon Gilmore and John Hemingway, Practical Gamma-ray Spectrometry, John Wiley and Sons Ltd, England (1995).

41. Technical Report Series No. 295, Measurement of Radionuclides in food and Environment, A Guidebook, IAEA, Vienna (1989).

42. P. Body, E.L. Hoffman, R.M. Lindstrom, S.J. Parry and R.J. Roserberg, Practical Aspects of Operating a Neutron Activation Laboratoy, IAEA-TEC DOC-564, Vienna (1990).

43. R.G. Helmer, R.J. Gehrke, R.C. Greenwood, Peak Position With Source Geometry in Ge(Li) Detector Spectra, Nucl. Instr. Methods, 123 (1975) 51-59.

44. A. Wyttenbach, Coincidence losses in Activation Analysis, Journal of Radioanalytical and Nuclear Chemistry, 8 (1971)335.

45. "Evaluated Neutron Data File, ENDF/B-V", ENDF/B Summary Documentation, compiled by R. Kinsey, ENDF-201, 3rd Edition, Brookhaven National Laboratory (1979).

46. L.R. Greenwood et al., Proc. 13th Int. Symposium (Part II) on Influence of Radiation on Material Properties, Philadelphia, ASTM STP 956 (1987) 743.

47. U. Garuska et al., INR-1871/I/PL/AU (1980).

48. A. Paulsen et al., Nucleonik, 10 (1967) 91.

49. G.N. Maslov, F. Nasyrov, and N.F. Paskin, Yad., Kanstanty, 9 (1972) 50.

50. C.M. Lederer, V.S. Shirley (Editor), Table of Isotopes, 7th Edition, John Wiley & Sons, New York (1978).

51. E.T. Cheng, D.L. Smith, Nuclear Data for Science & Technology, Proc. of an Int. Conf., held at the Forschungs Zentrum, Julich, Fed. Rep. of Germany, 13-17 May (1991) 273.

52. H. Vonach, The $^{27}Al(n,\alpha)^{24}Na$ Cross Section in Nuclear Data Standards for Nuclear Measurement, IAEA Tech. Report Series, 277 (1983) 59.

53. N.P. Kocherov et al., Proc. 7th ASTM EURATOM Symp. on Reactor Dosimetry, Strasbourg, France, Aug. 27-31 (1990) p.357.

54. T. Fukahori, JAERI-M 92-039 (1992) p114.

55. N. Kishida, Private Communication.

56. T. Nishida, Y. Nakahara, and T. Tsutsui, JAERI-M 86-116 (1986).

57. F. Atchison, Jul-Conf.-24 (1980).

58. K. Ishibashi, JAERI-M 90-025, (1990) p362.

59. Y. Nakahara and T. Nishida, JAERI-M 86-074 (1986).

60. N. Yamamuro, A Nuclear Cross Section Calculation System With Simplified Input-Format Version-I, (SINCROSS-I), JAERI-M 88-140 (1988).

61. S. Igarashi, "Program ELIESE-3; Program for calculation of the nuclear cross section by using local and non-local optical models and statistical model", JAERI 1224 (1972).

62. P.G. Young and E.D. Arthur, "GNASH: A Preequilibrium, Statistical Nuclear-Model Code for calculation of cross sections and emission spectra", LA-6947 (1977).

63. P.D. Kunz, "Distored Wave Code DWUCKY", University of Colorado (1974).

64. R.L. Walter and P.P. Guss, A Global Optical Potential Model for Neutron Scattering for A>53 and 10 MeV<E<80 MeV, Proc. Int. Conf. Nuclear Data for Basic and Applied Science, Santa Fe, New Maxico (1985) p.1079.

65. D. Wilmore And P.E. Hodgson, Nucl. Phys., 55 (1964) 673.

66. A. Gilbert and A.G.W. Cameron, Can. J. Phys., 43 (1965) 1446.

67. S.F. Mughabghab, M. Divadeenam, and N.E. Holden, "Neutron Cross Sections vol. 1, Neutron Resonance Parameters and Thermal Cross Sections Part A, Z=1-60" (1981).

68. S. Iijima, T. Yoshida, T. Aoki, T. Watanabe, and M. Sasaki, J. Nucl. Sci. Technol., 21 (1984) 10.

69. C. Kalbach, Z. Physik, A283 (1977) 401.

70. H. Kalka, M. Torjman, and D. Seeliger, Phys. Rev. C40 (1989) 1619.

71. H. Kalka, M. Torjman, H.N. Lien, R. Lopez, and D. Seeliger, Z. Phys. A 335 (1990) 163.

72. H. Kalka, Proc. of the 20th Int. Symp. on Nuclear Physics, Gaussig (1990).

73. H. Kalka, Z Phys. A (1990)

74. P. Ring and P. Schuck, The Nuclear Many-Body Problem, Spinger Verlag, New York, 1980.

75. A.B. Migdal, Theory of Finite Fermi Systems and Applications to Nuclei, Wiley Interscience, New York (1970).

76. F.A. Zhivopistsev and V.G. Sukharevsky, Phys. Elem. Part. Nucl. (Dubna), 15 (1984) 1208.

77. S.G. Kadmensky and P.A. Lukyanovich, Yad. Fiz. 49 (1989) 1285.

78. D. Agassi, H.A. Weidenmuller, and G. Mantzouranis, Phys. Rep. 22 (1975) 145.

79. T.A. Brody, J. Flores, J.B. French, P.A. Mello, A. Pandey, and S.M. Wong, Rev. Mod. Phys. 53 (1981) 385.

80. I.M. Green and Moszkowski, Phys. Rev. 139 (1965).

81. A. Faessler, Fortschr, Phys. 16 (1968) 309.

82. W. Dilg, W. Schantl, H. Vonach, and M. Uhl. Nucl. Phys. A 217 (1973) 269.

83. I. Angeli, J. Csikai, and A. Algora Pineda, Proc. of the 17-th Int. Symp. on Nuclear Physics, Gaussig, report zfk-646 (1987) 103.

84. A. Bohr and B.R. Mottelson, Nuclear Structure, Vol.2, Reading Benjamin (1975).

85. A. Chatterjee, K.H.N. Murthy, and S.K. Gupta, Pranama 16 (1981) 391.